MOLECULAR MECHANISMS UNDERLYING THE INHIBITORY EFFECT OF UNIAXIAL CYCLIC STRETCH ON ENDOTHELIAL CELL MIGRATION

by

Luis Cheng Sun

A thesis submitted to the faculty of
The University of Utah
in partial fulfillment of the requirements for the degree of

Master of Science

Department of Bioengineering

The University of Utah

December 2010

The University of Utah Graduate School

STATEMENT OF THESIS APPROVAL

The thesis of **Luis [redacted] Sun**

has been approved by the following supervisory committee members:

[redacted] Shiu	, Chair	**11-1-2010**
Brenda K. Mann	, Member	**11-1-2010**
[redacted] A. Weiss	, Member	**11-9-2010**

and by [redacted], Chair of

the Department of [redacted]

and by Charles A. Wight, Dean of The Graduate School.

ABSTRACT

Vascular endothelial cells in large arteries are constantly subjected to uniaxial cyclic stretch *in vivo* as a result of blood pressure's pulsatile nature. This thesis research aimed to understand the molecular mechanisms underlying the inhibitory effect of uniaxial cyclic stretch on endothelial cell migration in a wound healing scenario and with different wound directionalities. Our results showed that cyclic stretch decreased the migration speed in wounds with both long axes perpendicular and parallel to the stretch direction. This decrease in migration speed was significantly greater in perpendicular wounds than in parallel wounds, a finding that explains the potential importance of selective surgical incision directionalities to promote faster vascular wound healing.

In order to understand the possible mechanisms leading to the decrease of migration under cyclic stretch, the effects of uniaxial cyclic stretch on cell morphology and cytoskeletal remodeling, as well as the production of the pro-wound healing transcription factor ETS-1 and anti-wound healing excessive reactive oxygen species (ROS), were investigated. It was found that stretch did not affect cell area, which increased as the cells migrated into and covered a denuded region, thereby preventing the exposure of the thrombogenic vascular wall tissue to blood. However, stretch promoted the elongation and preferential alignment of cells perpendicular to the stretch direction. For subconfluent cells (e.g., such as those in a denuded area), the effect of stretch on

elongation and alignment was affected by the shape (i.e., the spatial boundary condition) of the denuded area. It was also found that stretch changed the focal adhesion dynamics (specifically, enhanced focal adhesions for adhesion and against migration) and decreased the amount of ETS-1. Both mechanisms may explain the decrease of migration under cyclic stretch. Although cyclic stretch induced the amount of intracellular ROS, ROS inhibitory studies, incorporating ROS scavengers and ROS generating enzyme inhibitors, showed neither reagent ameliorated recovery in cell migration.

Results from the hyperglycemia wound healing studies showed that hyperglycemia and cyclic stretch had additive effects on inhibiting endothelial cell migration through different mechanisms. Hyperglycemia hindered the increase in cell area in the wound zone, and ROS scavengers blocked the inhibitive effect of hyperglycemia on migration. These findings were the opposite of those in stretch experiments with normal glycemia as described above. Overall, the results explain the prolonged vascular injury and delayed wound healing in patients of hypertension (i.e., as approximated here by stretch) and hyperglycemia as well as suggest potential targets for developing new treatment to promote endothelial cell migration and wound healing in these diseased conditions.

TABLE OF CONTENTS

LIST OF FIGURES

ACKNOWLEDGEMENTS

First and above all I praise God. Without You, none of this would have been possible. I want to thank my parents and my sister Zuly for their unconditional love and support. No words could express my gratitude and what you guys have done for me. I would like to thank my thesis research advisor and supervisory committee chair Dr. Yan-Ting E. Shiu for her support and guidance. Dr. Shiu, thank you for the opportunity to work with you. You are a great scientist and through you, I learned to strive to do better in whatever I do. Thank you for your support and encouragement. I would like to thank Dr. Brenda K. Mann and Dr. Jeffrery A. Weiss for serving on my supervisory committee and giving me constructive feedback on my research. I would like to give thanks for the support and friendship from numerous people who worked or are working in Dr. Shiu's Vascular Bioengineering Laboratories. Specifically, I thank Dr. Matthew N. Iwamoto for helping me on the use of the stretch device; I thank Mr. Cole T. Quam, Mr. Jacob A. Jensen, and Mr. Jessie J. France for helping me on cell migration experiments; I thank Mr. Taylor J. Moore and Ms. Lindsey E. Corum for initiating the ETS-1 transcription factor study; I thank Ms. Jessica B. Sorensen for initiating the hyperglycemia study. Finally, I thank Dr. Bharat Jaishy for his friendship and feedback on conducting literature review during journal club meetings.

CHAPTER 1

INTRODUCTION

1.1 The Human Vasculature and Vascular Endothelium

1.1.1 Overview

The human vascular system comprises an extensive, complex network of arteries, veins, and capillaries that allow blood to reach the body's tissues and organs. The process of vascular development – angiogenesis – is a rigorously regulated process that has been thoroughly studied. In disease settings, such as cancer, tumors manipulate the vascular system for their own purposes. Angiogenesis represents a potential Achilles' heel for tumor growth because tumors depend essentially upon oxygen and nutrients carried, diffused, and filtered by the body's vascular system. In treating cardiovascular disease, including conditions such as acute myocardial infarction, angiogenesis can direct the growth of new blood vessels (27).

Researchers have focused on studying angiogenic signals in endothelial cells (ECs), which line the lumen or innermost interior layer (tunica intima) of blood vessels, that effectively work to separate the circulating blood from underlying vascular tissues and perform numerous functions, including, among other things, cell migration, remodeling, proliferation, apoptosis, and the regulation of contractility of vascular

smooth muscle cells. The shapes and functions of ECs differ among the three types of blood vessels. In capillaries, the ECs are flatter and more elongated than in arteries and veins, which are thicker and polygonal. The thin EC barrier in capillaries regulates exchanges of nutrients while the thicker EC monolayer in arteries and veins has a role in regulating, among others, blood pressure and the normal cycle of heart contraction (5). ECs are constantly exposed to hemodynamic stresses such as fluid wall shear stress and pulsatile pressure-induced cyclic stretch.

1.1.2 Cell-Cell Junctions: Adherens Junctions

Endothelial cells lining the vessel wall are connected by adherens junctions, tight junctions, and gap junction, of which adherens junctions are most essential in controlling cell migration. Adherens junctions, which both mediate cell adhesion and support key molecular interactions for cell-to-cell contact, are formed by members of the cadherin family of adhesion or transmembrane proteins, including cadherins, α-catenin, β-catenin, and γ-catenin. Endothelial cells express relatively high levels of two cadherins: a cell-type-specific cadherin called vascular endothelial (VE)-cadherin, and neuronal cadherin (N-cadherin) that is also present in other cell types such as neural cells and smooth muscle cells (3). Cadherins, which can be further be divided into Type I and Type II subfamilies, also play an extensive set of cellular-specific roles, including cell recognition and sorting, cytoskeletal organization, cell migration, cell proliferation, and cell survival. Their functional versatility is facilitated by their capacity to trigger signal transduction in the cytoplasm and through interactions in intracellular domains involving

cytoskeletal regulators, transcription protein factors, and other intercellular binding partners (3).

1.1.3 Focal Adhesions: Integrin and Vinculin

In order to maintain structural integrity, ECs must be anchored to their substrate in order to survive and proliferate, suggesting signals mediated by the integrin-family of adhesion receptors are essential in regulating EC function (17, 23, 38-40). As a cell-surface receptor essential in growth, immune response, and wound healing, integrins consist of two glycoprotein subunits or chains, which extend across the cell membrane connecting the inside of the cell to the outside. These subunits – the alpha and beta chains – contribute to the binding process. Many types of integrins exist and cells may have multiple types on their surface. Integrins can bind to one or multiple partner ligands principally found in the external cellular environment (i.e., extracellular matrix molecules). Thus, integrin-ligand interaction can have very high specificity as, for example, with $\alpha_6\beta_4$ binding to laminin in epithelial cells or multiple ligand binding specificity as with $\alpha_v\beta_3$ interacting with Cyr61, fibronectin, fibrinogen, osteopontin, and vitronectin in glioblastoma, melanoma, and activated endothelial cells. Ligand binding to integrins results in clustering of integrins and subsequent recruitment of actin filaments to the integrin cytoplasmic domains. This recruitment process is facilitated by a group of interacting cytoskeletal proteins, including α-actinin, filamin, talin, and vinculin. Integrins convey tractional forces developed in the cytoskeleton to the extracellular matrix (ECM) and stresses applied to cells from the ECM. In order to form effective cell-to-cell or cell-to-extracellular matrix contacts, several integrins must be localized at the

focal contact. When integrins are diffusely distributed over cellular surfaces, no strong adhesion will be present, but their weak affinity for ligands is necessary to prevent irreversible binding of cells that otherwise would result in a lack of cell migration.

Recruitment of talin, vinculin, and kinases also closely correlates with increased adhesion strength. For example, membrane cytoskeletal linker protein, such as vinculin, facilitates a cell's capacity to move through its environment, by connecting the actin cytoskeleton to integrin's cytoplasmic domain at sites called focal adhesions (FA). Although vinculin does not link integrins directly, vinculins have been shown to play a key role in FA assembly by indirectly binding to talin and α-actining and recruiting additional proteins such as paxillin and vinexin (2, 43).

1.2 Hemodynamics Stresses

ECs, as a result of their unique locations, are bombarded continuously by various mechanical stresses, including pressure-induced cyclic stretch and fluid wall shear stress. Pressure-induced cyclic stretch is defined as a regularly repeated change in lumen diameter caused by the pressure gradient between the vessel lumen and its exterior. *In vivo*, blood flow is not uniform throughout the body and, thus, fluid shear stress is not constant but, rather, it varies depending on the cardiac cycle. In arteries, the normal flow pattern is laminar with secondary flows generated at curves and branches (i.e., bifurcations). At these bifurcation points, velocity profile skewing sometimes can create pockets in which wall shear stress is low and oscillates in different directions. As a result, blood flow patterns change from laminar to disturbed (22). Some studies correlated early vessel thickening in arteries with low and oscillating wall shear stress

(37). Atherosclerosis has also been shown to form preferentially in the outer wall of these branch points where vessels experienced a combination of low levels of shear stress and high levels of cyclic strain. These stresses affect a wide array of EC function and behavior, including cytoskeletal organization, gene expression, proliferation, and migration (14).

Evidence continues to accumulate indicating that the externally applied cyclic stretch regulates cytoskeletal organization, cell morphology, signal transduction, gene expression, and EC functions, including angiogenesis and wound healing (7). As the endothelium in the body's vascular system is constantly subjected to the forces of a complex mechanical environment, the challenge for researchers is to recreate a physiologically more relevant *in vitro* mechanical environment for investigating the effects of various stresses on EC. These have included uniaxial and biaxial devices (8, 19).

1.3 Cell Migration

Vascular ECs, with their tight inner-wall barrier separating the blood flow and the subendothelial tissue, need to have adequate motility, which is important to virtually every physiological and pathological process (e.g., loss of ECs as a result of surgery or inflammation, atherosclerosis, wound healing, embryonic morphogenesis, cancer metastasis) (13). An intact endothelial cell monolayer is essential for maintaining vascular homeostasis and guiding remolding and vascular repair. The dynamic process of cell migration is cyclically driven by both actin-polymerization and de-polymerization. EC migration initiates with the extension of protrusions at the cell front by polymerizing

actin, leading to its subsequent attachment to the substratum. This process is followed by actomyosin filament contraction at the front of the cell to pull the body forward and toward the protrusion. The cycle completes when adhesive connections in the rear of the cell release and retraction of the tail occurs. The orchestration of each cycle is initiated by external signals (i.e., chemotactic molecules). In summary, EC migration begins with carefully timed cytoskeletal organization (i.e., the forward translocation of the cellular body), and, most critically, the initial step of change coordination in cell adhesion (i.e., the extension of the leading edge and its adhesion to the substrate) (13). FAs, the cell-matrix contact sites where integrins bind to the ECM externally and bind to cytoskeleton internally, form so that a cell can migrate more quickly and freely. Although fluid shear stress is a well-established continuous stimulus for ECs and serves to regulate EC migration (13), the effect of cyclic stretch on EC migration has yet to be as extensively investigated (28).

1.4 Vascular Wound Healing and Endothelial Migration

Compromised endothelium integrity, such as a loss of ECs due to inflammation or surgery, can lead to such vascular disorders as thrombosis, atherosclerosis, and stenosis, particularly when the denuded area is not restored in a timely manner (13, 29). In order for a "wound" (that is, an area denuded of ECs) to be closed rapidly, rapid repair generally occurs through the migration of adjacent ECs into the denuded area; proliferation may be required if the size of the denuded area is significant enough to have an impact upon normally expected healing progress. Proliferation of endothelial cells in wound healing normally occurs between 6 to 8 hours after the initial process of

migration. The physical process involved in EC migration consists of cycles of (a) membrane protrusion at the leading edge, the formation of FAs at the cell front, and its adhesion to the extracellular matrix molecules; (b) the generation of intracellular contractile force by the actin-myosin cytoskeleton, which is transmitted via cell-ECM adhesion sites to the underlying substrate as a traction force for propelling the forward translocation of the cell body; and (c) the release of cell-extracellular matrix adhesions at the rear (13).

1.5 Cell Morphology

Along with fluid wall shear stress, pulsating blood flow also generates a cyclic circumferential strain (i.e., hoop stretch) along the entire arterial wall. Both have known to affect EC morphology.

1.5.1 Effects of Fluid Shear Stress

When exposed to steady laminar shear stress, endothelial cells will flatten, elongate, and align parallel to the flow direction. However, oscillating flow completely inhibits this morphological response and endothelial cells are rounded. The effects of steady and oscillating flow on EC morphology have been found *in vivo* in areas where the respective flow patterns would occur and also have been replicated through *in vitro* experiments (42).

1.5.2 Effects of Stretch

This cyclic stretch effect also induces endothelial cells to undergo cell

morphology changes *in vitro*. Endothelial cells – cultured on deformable surfaces such as silicone rubber membrane – adapt to continuous cyclic stretch (e.g., created by a vacuum or motor) by elongating and aligning transversely to the direction of stretch. The substrate deformation may result in nonuniform elongation, especially in biaxial stretch devices. In addition, with most stretch devices, oscillating flow is observable from the liquid nutrient medium overlay that may move concurrently with the deformation of the membrane (8, 19, 28).

1.5.3 Effects of Combined Shear Stress and Stretch on Cells in a Blood Vessel Wall

Separate studies have shown that shear stress and cyclic stretch induce actin microfilaments to rearrange into stress fibers that are preferentially aligned with the long axis of the cells. If a blood vessel is approximated to have a cylindrical geometry – that is, shear stress is in the axial direction and stretch is mainly circumferential – this then means cells and stress fibers should align parallel to the long axis of the tube. In other words, this will be in the same direction as under unidirectional shear stress.

However, looking at the effects of each force component separately is particularly challenging in understanding how these stimuli – which *in vivo* depend on flow, blood pressure, and vessel wall structure – interact to trigger complex cellular responses. Cellular structural integrity initiated by cyclic stretch may be the mediating factor in the process of remodeling the cytoskeleton, but the literature has not yet clearly indicated what threshold levels of cyclic stretch are critical to endothelial cell morphology. Furthermore, any discrepancies in reported data would be hard to reconcile, depending

upon many factors, such as whether stretch devices incorporated pulsatile pressure–induced uniaxial cyclic stretch rather than the more commonly used approach of biaxial stretch directly imposed on the substratum. Other factors include cell type, frequency and type of stretch, and length of experimentation.

1.6 Reactive Oxygen Species and Hyperglycemia

1.6.1 Reactive Oxygen Species

Reactive oxygen species (ROS) play key roles in routine physiological and cellular processes, including signaling, angiogenesis, growth, and homeostasis. The vascular endothelium also is vulnerable to injury because of oxidative stress, either imposed from external or internal sources. Along with elevated levels of free radicals, ROS excess and diminished nitric oxide (NO) bioavailability are relevant in chronic disease conditions, including cardiovascular and kidney disease, advanced glycosylation end product (AGE)-related diseases, and insulin resistance (such as Type II diabetes) (43).

Although physiological levels of ROS are critical in cell signaling, an excess of ROS or their inadequate metabolism can induce oxidative stress. ROS are generated by oxidative cellular processes, principally by NAD(P)H oxidase, endothelial nitric oxide synthase (eNOS), xanthine oxidase, and mitochondrial electron transport. ROS are then metabolized to hydrogen peroxide (H_2O_2) by dismutation of superoxide (O_2^-) by superoxide dismutase (SOD) and converted to water principally by glutathione peroxidase (GPx) and catalase (43). Most of ROS is generated by the mitochondria. While there is evidence that ROS can be produced in extra-mitochondrial sites and under

anaerobic conditions, further research is still needed to identify the underlying mechanisms of these ROS' role in various disease settings. Studies have also shown that cyclic stretch stimulates ECs to increase ROS production (12, 21).

1.6.2 Hyperglycemia

Normal glucose levels range from 70-120 mg/dl (0.7 – 1.2 mg/ml), and after meals glucose levels range from 120-200 mg/dl (1.2 – 2.0 mg/ml). For uncontrolled conditions of diabetes, levels can range from 300-600 mg/dl (3.0 – 6.0 mg/ml). A polar and hydrophilic molecule, glucose comes in two forms. Cells cannot metabolize L-glucose. ECs uptake D-glucose based on an external environmental concentration gradient, or cellular demand, mainly through two transporters for energy and metabolism: glucose uniporters and sodium-powered glucose symporters (45). Cells normally uptake glucose molecules and break them down into pyruvate molecules through the glycolysis pathway in the cytosol. They are then taken into the mitochondria and run through the citric acid cycle in which the final products of water, carbon dioxide, and ATP are formed.

Hyperglycemia occurs in cases when the glucose amount absorbed by cells is hindered by a decrease of cell membrane bound receptors, which, in turn, leads to higher glucose concentrations in the blood. The higher glucose concentrations in blood could drive glucose modules through diffusion into the cell. Normally, cells break glucose down through the oxidative cycles of glycolysis and citric acid cycle. With increased numbers of glucose molecules inside the cytoplasm, structures inside the cell can become glycated through nonenzymatic glycosylation (45), which, in turn, could alter the

cytoskeleton and focal adhesions (FAs) and slow the rate at which ECs migrate. The result is a decrease in cell motility and accelerated rate of cellular death (1, 15, 32).

For patients with diabetes, potentially fatal cardiovascular complications become prevalent possibly due to the elevated glucose amounts in the bloodstream. Hyperglycemic conditions have been linked to the development of atherosclerosis, though its underlying causes and triggers have yet to be fully understood. Higher glucose concentrations inside or outside the cellular matrices can lead to various hyperglycemic induced pathways: activation of the aldol reductase pathway, advanced glycation end-product pathway, the protein kinase C pathway, or ROS intermediate pathway. These pathways could damage cells and severely impair their function, including conditions, to name a few, of hyperpermeability, basement matrix thickening, thrombosis, abnormal blood flow, and abnormal cell growth (41).

1.6.3 Antioxidants

Antioxidants, which decrease the amounts of free radicals by inhibiting ROS generation or converting them into stable molecules (i.e., paired electrons in open shell configuration), can help patients showing high glucose levels (30, 31). While excessive levels of ROS have negative impacts upon cell function and viability, normally low physiological levels of ROS have been shown to be essential to various signaling pathways and optimal cell function (18, 34, 35). Researchers have yet to fully explain the underlying mechanisms that would implicate the importance of endogenously produced ROS in hyperglycemia-related conditions, and the extending idea that normal, limited

ROS production is key to normal physiological functions in the vasculature and surrounding body and organ tissue.

Research has shown that N-Acetyl-L-Cysteine (NAC), a ROS scavenger, is capable of blocking contraction-mediated glucose transport. Diphenyleneiodonium (DPI), a potent ROS inhibitor that blocks several cellular oxidase systems, including NAD(P)H oxidase, endothelial nitric oxide synthase (specifically, for the regulatory purposes of balancing and avoiding abnormally proliferating production), mitochondral Complex I, and xanthine oxidase, is useful in improving chronic conditions such as vasoconstriction, endothelial dysfunction, kidney dysfunction, and hypertension and has some clinical usefulness in hyperglycemia (43).

1.7 Transcription Factor: ETS-1

The selection of a tip cell, the first cell emerging from the parent blood vessel, is a crucial early step in sprouting angiogenesis where ECs develop and differentiate and begin to migrate as the cell junctions destabilize and the extracellular matrix accommodates the invasion of the ECs into surrounding body and organ tissues. As the new adult blood vessels form, the cellular matrix interactions stabilize and EC homeostasis is once again achieved. Among the wide arrays of the molecular pathways regulating the formation of new blood vessels, a network of ETS transcription factors assume critical roles not only in cellular growth, survival, and homeostasis, but also in the process of wound healing and in diseases where cancer and inflammation are present (9, 10, 20).

The ETS-1 transcription factor, the primary member of the ETS protein family, has been studied extensively. ETS over-expression, for example, increases angiogenic responses and up-regulates stimulators such as vascular endothelial growth factors. Levels of the ETS transcription factors found in ECs could likely be affected by shear stress or cyclic stretch. While researchers have yet to conclude whether ETS transcription factors in ECs are mechanically sensitive, there is evidence that ETS-1 is modulated by activated MAP kinase and ERK1/2 pathways, both of which have been determined to be mechanically sensitive (13).

1.8 Aims and Hypotheses of this Study

The overall goal of this thesis is to investigate the molecular mechanisms underlying the effect of cyclic stretch on EC migration. The hypothesis is that stretch inhibits EC migration via hindering morphological/cytoskeletal remodeling that is required for migration to take place, inhibiting the generation of ETS-1, and/or stimulating excessive ROS generation. Also tested is the hypothesis that stretch and hyperglycemia have an additive effect on inhibiting EC migration by enhancing the negative morphological remodeling and/or ROS pathway.

CHAPTER 2

MATERIALS AND METHODS

2.1 Routine Endothelial Cell Culture

Bovine Aortic ECs (BAECS) (Cambrex Corp; East Rutherford, NJ) were cultured in 100-mm Petri dishes in Dulbecco's Modified Eagle Medium (DMEM) (Gibco/Invitrogen; Carlsbad, CA) and supplemented with 5% Fetal Bovine Serum (FBS) (Hyclone; Logan, UT), 1% Sodium Pyruvate (Gibco/Invitrogen), and 1% Penicillin-Streptomycin (Gibco/Invitrogen). Cultures were maintained in a controlled environment at 37°C using a humidified 5% CO_2-95% air incubator (Forma Series II, Thermo Scientific; Waltham, MA) prior to cell seeding onto stretch templates as described below. Cell passages 8-12 were used for the experiments.

2.2 Fibronectin-coated Silicone Membrane Preparation and Assembly

Medical-grade silicone rubber sheets (0.01" thick, 40 Durometer Gloss/Gloss) (Specialty Manufacturing; Saginaw, MI) were cut to desired dimensions: 4 cm x 6 cm (W x L) and assembled into custom-built polycarbonate cell stretch templates and chambers as described in Joung et al. (27). Polycarbonate templates and stretch chambers were cleaned by sonication (Bransonic 3510, Emerson Industrial Automation; Danbury, CT)

with a mixture of water-soap solution (Haemo-Sol Regular; Baltimore, MD). Subsequently, all materials were sterilized either by autoclaving (2340M, Tuttnauer; Hauppage, NY) or by soaking in 70% ethanol for a 30-min period. Materials were then air dried under UV radiation for 20 min in a biosafety cabinet (Forma Class II A/B3, Thermo Scientific; Waltham, MA).

Previously, strain analysis incorporating a Lagrangian Strain Tensor program indicated cells in the center region of silicone rubber sheets were exposed in a predictable and homogeneous strain field with negligible lateral thinning (Joung, Iwamoto et al. 2006). Therefore, cells were seeded in the center region for the current experiments. A silicone rubber gasket (2.5 cm x 2.5 cm) with an inner cutout of 2 cm x 2 cm was placed on top of the center region. A 5 $\mu g/cm^2$ fibronectin solution (Sigma-Aldrich; St. Louis, MO) was allowed to absorb into this restricted section in the silicone rubber membrane for 2 h at room temperature inside a biosafety cabinet. Fibronectin-coated membranes were then washed twice with phosphate buffer saline (PBS) (Gibco/Invitrogen) solution to remove any unbound fibronectin and to ensure specific cell-ECM binding. The gasket also served to confine cell distribution to the center region.

2.3 Wound Healing Model and Cell Stretching Experiments

At $3x10^4$ cells/cm^2 density, BAECs were seeded onto the 5 $\mu g/cm^2$ fibronectin-coated silicone rubber sheets. Cells were cultured with supplemented DMEM and under a controlled environment as described above. Upon confluence (i.e., approximately 48 h), BAECs were used in migration studies within 24 h.

EC strips (10 mm long, 200 μm wide) were manually removed from the cell monolayer using a commercially available scraper (Fisher Scientific; Pittsburgh, PA). The long axis of these wounds (i.e., EC denuded areas) was either perpendicular or parallel to the uniaxial stretch direction. Immediate after wounding, cell media were replaced. The injured EC monolayers were kept as static controls or cyclically stretched at 20% membrane elongation and a frequency of 1 Hz (i.e., 60 c.p.m.) for 3 h (Figure 2.1). In all experimental conditions, BAECs within the cell stretching device were maintained constantly at 37°C. The cell stretching system also delivered humidified 5% CO_2-95% air gas mixture directly to the stretch chambers where cells were maintained. The constant supply of the gas mixture sustained the cell culture medium (i.e., supplemented DMEM) at a constant physiological pH (~7.3-7.4).

2.4 Microscopic Phase Contrast Image Acquisition

Images showing phase contrast images of cell monolayer wounds were recorded immediately after strips of ECs were removed (time = 0) and again at the end of the experiments (time = 3 h). Images were acquired with an inverted microscope (IX70, Olympus; Center Valley, PA) equipped with a 10x and 20x objective, and a cooled CCD camera (ORCA-ER, Hamamatsu; Bridgewater, NJ) by using a commercial imaging software (IPLab, Scanalytics; Fairfax, VA). Phase contrast micrographs of the wounds were acquired and transferred directly from frame grabber to computer storage.

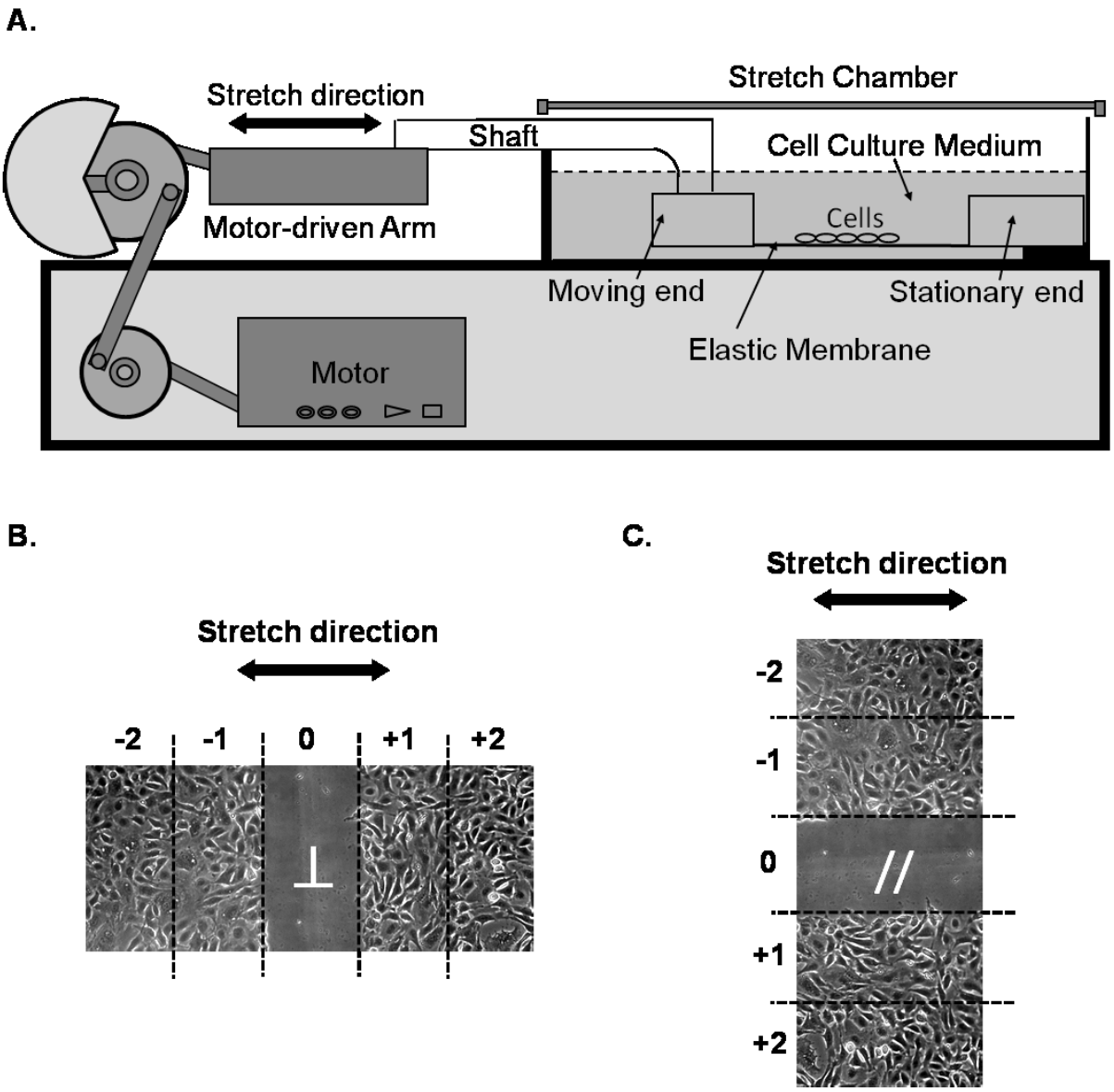

Figure 2.1 Wound healing and stretch experiments. (A) Uniaxial Cell Stretch Device. A custom-designed cell stretch device was used to impart cyclically controlled membrane elongation (20% at 1 Hz) to a silicone rubber sheet seeded with endothelial cells. **(B)** Perpendicular Wound. The long axis of the cell denuded area was perpendicular (⊥) to the uniaxial stretch direction. **(C)** Parallel Wound. The long axis of the cell denuded area was parallel (//) to the uniaxial stretch direction. In **(B)** and **(C)**, each microscopic image of the wound area was divided into 5 distinct regions for morphological analysis: the wound zone (~200 μm wide by 10 mm long and labeled as "0"), two 0-200 μm wide zones away from the wounded area (i.e., one at either side of the wound and labeled as "+1" and "-1"), and two 201-400 μm wide zones away from the wounded area (i.e., one at either side of the wound and labeled as "+2" and "-2").

2.5 Cell Migration Speed Analysis

The differential width (i.e., change in wound sizes) of the wounds was calculated from images containing the widths of the denuded areas at time 0 and 3 h using the IPLab imaging software and a custom-written Visual Basic program in Excel (Microsoft; Redmond, WA). The migration speed was then calculated as the change in the wound size divided by experiment time (i.e., 3 h) and by 2 (i.e., taking into account migration proceeds from both sides of the wound). Migration speed was expressed in units of micrometers per hour (μm/h). Each experiment had triplicate samples, and at least three independent experiments ($N \geq 3$) were conducted for each condition (i.e., static and 20% strain).

2.6 Cell Morphology Analysis

Several morphology features, including area, perimeter, shape, and orientation, were quantified using the same phase contrast images for migration analysis and the IPLab software. Each wound image was divided into 5 distinct regions: the wound zone (~200 μm wide by 10 mm long and labeled as "0"), two 0-200 μm wide zones away from the wounded area (i.e., one at either side of the wound and labeled as "+1" and "-1"), and two 201-400 μm wide zones away from the wounded area (i. e., one at either side of the wound and labeled as "+2" and "-2") (Figure 2.1). Boundaries of randomly selected cells in each zone were manually traced and then used to calculate area (μm^2), perimeter (μm), major and minor axes (μm), and orientation (°) of individual cells using IPLab. Specifically, axes were determined by fitting the cell boundary into a best fitted-ellipsoid generated from the imaging software (Figure 2.2A). The shape of cells was determined

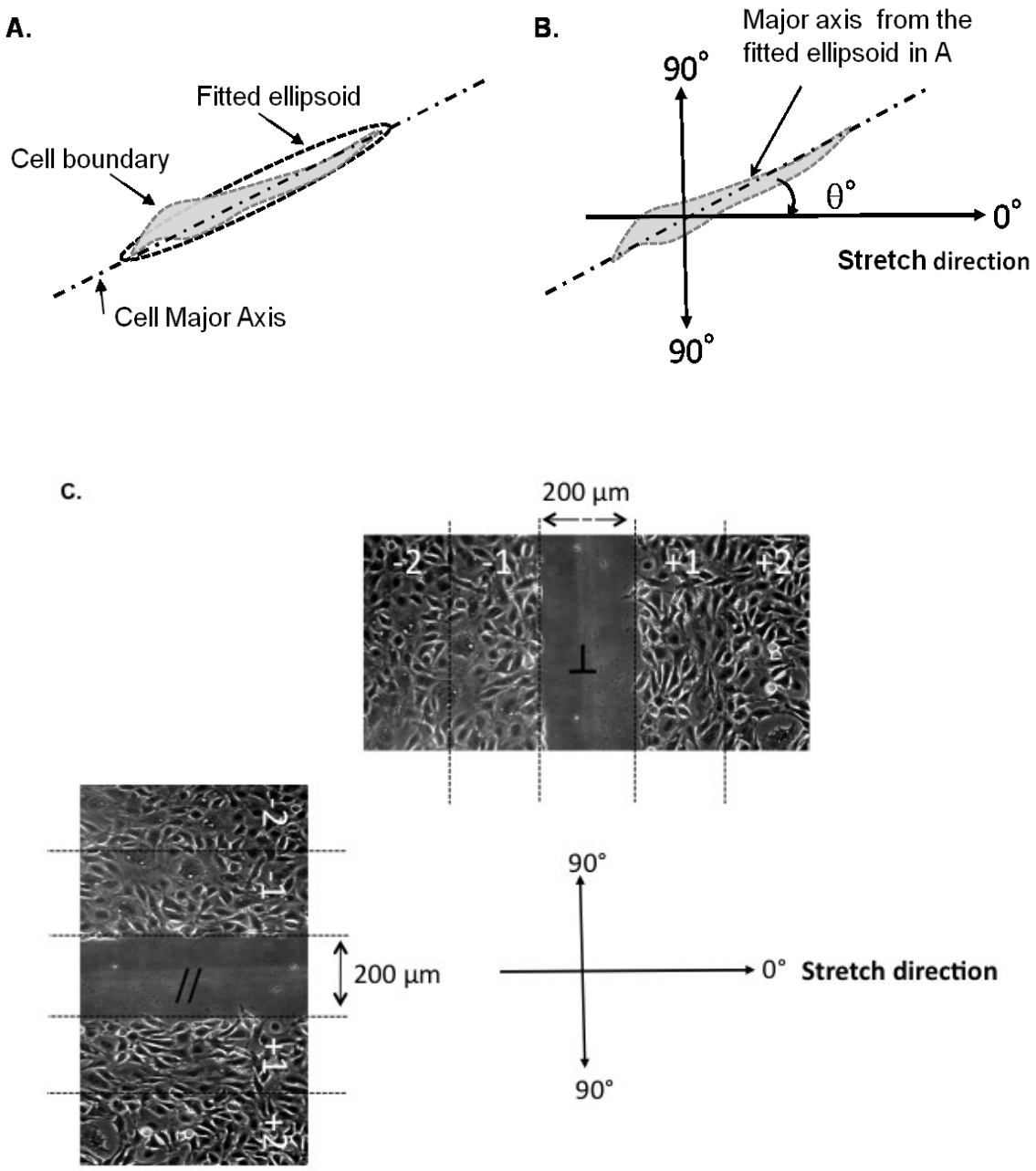

Figure 2.2 Morphological features approximated through computer analysis. (A) Major axis of cells was determined by individually tracing and fitting the cell boundary into a best fitted-ellipsoid. This fitted-ellipsoid was also used for measuring cell orientation under cyclic stretch **(B)**. The overall cell orientation is the angle (θ°) between the major axis of the best fitted-ellipsoid and the axis of parallel to the direction of stretch (set to be 0°). **(C)** Stretch directions were set to be 0°. Wounds were made parallel (//) or perpendicular (⊥) to the direction of stretch. Five zones of 200 µm were established.

as the ratio of the long axis over the short axis. In other words, a cell ratio of 1:1 results in a perfect cellular sphere.

The overall cell orientation is the angle (θ) between the major axis of the best fitted-ellipsoid and the axis parallel to the direction of stretch (set to be 0°) (Figure 2.2B). Cell angles were grouped into three categories: <30°, ≥30° to <60°, and ≥60° to ≤90°. The overall orientation of cells was expressed as percent angle distribution between the major axis of its best-fitted ellipsoid and the axis parallel to the stretch direction. A total of 75 cells were selected arbitrarily within each zone, comprising a total of 375 cells per micrograph. Three representative images were selected per each experimental condition (i.e., static and stretch, parallel and perpendicular wounds) at times 0 and 3 h. Each experiment had triplicate samples, and at least three independent experiments ($N \geq 3$) were conducted for each condition. Since there were no cells left after wounding in zone "0", comparisons of the EC's morphological characteristic at time 3 h after were made based on the average properties (i.e., average values across cells in neighboring regions) of cells in the adjacent zones. This method is a fair approximation-model because these are the same cells migrating into the denuded area.

2.7 Fluorescent Immunostaining of Cell Nuclei, Cell-Cell Junctions, Focal Adhesions, and Actin Filaments

At the end of each experiment, cells were washed three times with PBS to remove any residual serum and then fixed with 3.7% formaldehyde (Sigma-Aldrich) for 15 min. Cells were then permeabilized with 0.1% Triton X-100 (Sigma-Aldrich) for another 15 min. In staining for cell nuclei and F-Actin filaments, cells were incubated with Hoechst

33342 dye and Phalloidin tagged with Alexa fluoro 488 for 30 min. In staining for vascular endothelial (VE)-cadherin cell-cell junctions, cells were incubated with goat polyclonal anti-VE-Cadherin primary antibody (1:100) (Santa Cruz Biotechnology; Santa Cruz, CA) for 1 h, followed by incubation in the dark with rhodamine-tagged donkey anti-goat secondary antibody (1:500) (Santa Cruz Biotechnology) for 30 min. In staining for focal adhesion protein, cells were incubated with mouse monoclonal anti-vinculin primary antibody (1:100) (Sigma-Aldrich) for 1 h followed by FITC-conjugated bovine anti-mouse secondary antibody (1:500) (Sigma-Aldrich) for 30 min in the dark.

After incubation, fluorescently labeled cellular structures were observed under an inverted microscope (IX70) equipped with epifluorescence optics and a 20x objective as well as under a confocal laser scanning microscope (Olympus FV1000) equipped with 40x and 60x objectives. The excitation/emission wavelengths for F-actin filaments and nuclei were 495/518 and 350/461 nm, respectively. The excitation/emission wavelengths for VE-cadherin and vinculin were 535/565 nm and 470/505 nm, respectively. Fluorescent images were acquired using a cooled CCD camera as described above.

2.8 Staining of ETS-1 Transcription Factor in Endothelial Cells

Rabbit anti-ETS-1 antibody (primary 1:100) and rhodamine-tagged goat anti-rabbit antibody (secondary 1:500) were used to obtain ETS-1 stained fluorescent microscopic images. Mean fluorescent ETS-1 intensities of static and stretched BAECs in the nucleus and cytosol at 0 and 3 h were determined using the ImageJ software (NIH). The noncellular intensity (i.e., background) of an area of equal size nearby the selected cell was determined for background intensity. A “net” ETS-1 intensity indicating the

amount of ETS-1 present in cells was obtained by subtracting the background intensity from the intensity of specific cell compartments (i.e., nuclear and cytosolic). Three independent experiments were carried out for each condition (i.e., static versus 20% stretch) and the same time points (0 and 3 h). Three representative images were selected per condition and time point and a total of 30 cells were randomly selected per image.

2.9 Fluorescent Immunostaining of Intracellular Reactive Oxidation Species

Intracellular ROS levels were detected using a fluorescent probe, 5-(and-6-) chloromethyl-2',7'-dichlorodihydrofluorescein diacetate, acetyl ester (CM-H_2DCFDA) (Molecular Probes; Eugene, OR) as described previously (36). Following stretch experimentation, the cells were washed three times with warm PBS and then incubated with the probe (final concentration of 13 μM) for 30 min at 37^{o}C in the dark. The cells were then washed three times with PBS, fixed in 3.7% formaldehyde, and observed under fluorescence microscope. Fluorescent images of cells in and adjacent to the denuded area, once again, were acquired as described above.

The ROS dye excitation/emission wavelengths were 470/505 nm. Cellular outlines were traced and the cell body's internal fluorescence intensity was measured with IPLab as was the intensity of a noncellular area of equal size nearby the cell for the purposes of establishing background intensity. The cell's intensity measurement was subtracted from the background intensity measurement, yielding a "net" intensity indicating the level of ROS. In each experiment, the "net" cellular intensity of stretched samples was normalized to static controls level. Each experiment had duplicate or

triplicate samples, with each condition (i.e., static versus stretch) having more than 50 cells pooled from each of the three independent experiments.

2.10 Removal of Intracellular Reactive Oxygen Species

Antioxidant N-Acetyl-L-Cysteine (NAC, 20 mM) (Sigma-Aldrich; St. Louis, MO), a nonspecific ROS scavenger that inhibits activation of c-Jun N-terminal kinase, p38 MAP kinase, redox sensitive activating protein-1, and NF–KB transcription factor, was used as a free radical scavenger to remove intracellular ROS amounts. Flavoprotein inhibitor DiPhenylene Iodonium (DPI, 10 μM) (Sigma-Aldrich; St. Louis, MO) was also used to inhibit ROS production. DPI is a potent, specific ROS inhibitor that blocks several cellular oxidase systems, including NAD(P)H oxidase, endothelial nitric oxide synthase, mitochondral Complex I, and xanthine oxidase. BAECs were cultured on fibronectin-coated silicone rubber membranes and cells were allowed to reach confluence and then incubated with NAC or DPI for 1 h prior to wound healing/migration studies. Wounded ECs were kept as controls or cyclically stretched at 20% membrane elongation at 1 Hz for 3 h. Cell migration speed of static controls and stretch samples were calculated as described previously.

2.11 Hyperglycemia Wound Healing Model and Stretch Experiments

Cells were cultured under hyperglycemia (HG, glucose concentration = 4.5 g/L) and normglycemia (NG, glucose concentration = 1 g/L) media before experimentation for 2 days. Using a cell scraper, three wounds were incised on each of the templates. Samples were classified into 4 groups: HG stretch, NG stretch, HG static, and NG static

controls. Immediately after wounding, the templates were photographed and then subjected to either cyclic stretch or static environments for 3 h. Migration and morphology analyses were performed as described above.

2.12 Fluid Agitation Experiments

Fluid oscillation experiments were performed to rule out any fluid shear effects on ECs created by media agitation with the cycling of the moving shaft in our stretch system. In these motion controls, the polycarbonate templates were not fixed at the stationary end and were attached only to the shaft in the moving end, thus resulting in free movement for the entire polycarbonate template. The silicone membranes in motion controls samples were displaced without being stretched for an identical distance and frequency as their stretched counterparts. This setting provided a control for the effect of fluid motion over the surface of ECs generated by the moving shaft in contact with the surrounding media (11).

2.13 Data Presentation and Statistical Analysis

Student's t test and ANOVA ($p < 0.05$) were used to determine significant difference between two and more than two sets of data, respectively. Each experiment had triplicate samples, and at least three independent experiments ($N \geq 3$) were conducted for each condition. Data are presented as mean ± standard error of the mean (SEM).

CHAPTER 3

RESULTS AND DISCUSSION

3.1 Cyclic Stretch Decreases the Migration Speed of ECs in Different Wound Directionalities

EC migration under uniaxial cyclic stretch was investigated in an *in vitro* wound healing scenario where wounds were created in both directions with long axis perpendicular (Figure 3.1) and parallel (Figure 3.2) to the stretch direction. Injured EC monolayers were exposed to 20% membrane elongation stretch at 1 Hz for 3 h or kept at static controls. Phase contrast images of wounds were acquired with a microscope coupled with a video camera capable of rendering still and real time images. These "wound" images were used to determine the change in wound sizes and subsequently to calculate EC migration speed via imaging analysis software. ECs aligned perpendicular to the stretch direction, and the direction in which wounds were created did not affect this preferential perpendicular alignment of ECs under cyclic stretch observed in many other studies (i.e., ECs aligned perpendicularly to the stretch direction in both "perpendicular and parallel wounds"). The average EC migration speeds under static conditions were 27.58 μm/h and 30.53 μm/h (difference was not statistically significant) for perpendicular and parallel wounds, respectively. Under stretch conditions, the average EC migration

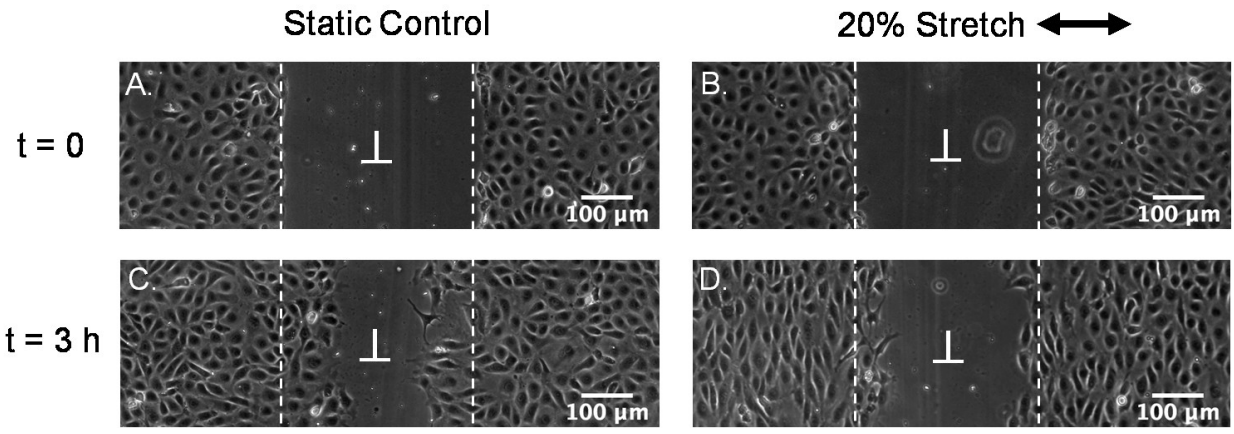

Figure 3.1 Representative microscopic images of perpendicular (⊥) wound healing under stretch. A static control sample at t=0 **(A)** and 3 h **(C)**, and a 20% stretch sample at t=0 **(B)** and 3 h **(D)**. Double headed arrow indicates stretch direction.

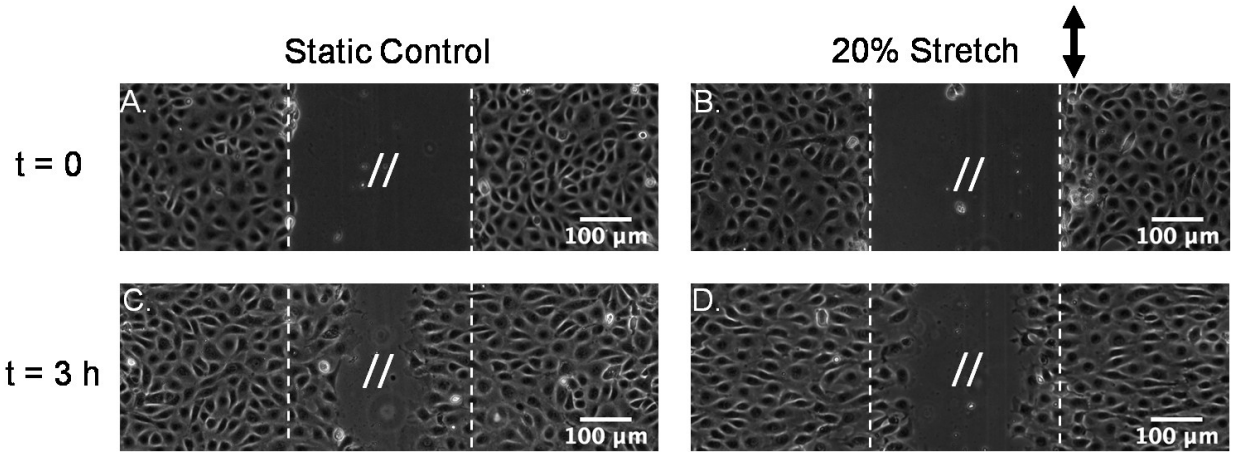

Figure 3.2 Representative microscopic images of parallel (//) wound healing under stretch. A static control sample at t=0 **(A)** and 3 h **(C)**, and a 20% stretch sample at t=0 **(B)** and 3 h **(D)**. Double headed arrow indicates stretch direction.

speeds decreased to 17.58 μm/h and 25.94 μm/h for perpendicular and parallel wounds, respectively. In summary, a 36% decrease in migration speed was observed in wounds with long axis perpendicular to the direction of stretch and a 15% decrease for wounds with long axis parallel to the direction of stretch (Figure 3.3A).

The differential decrease in migration speed may be related to, among other things, the directionalities in which wounds were created and the ability of stretched cells to adapt or regulate morphological changes under strain. In order for nearby cells to migrate toward the wound site and to cover the wound quickly, cells should develop a polarized shape where the long axis connecting the front (i.e., lamellipodia) and the end (i.e., the tail) of a cell is perpendicular with the long axis of the wound (Figure 3.3B). In the experimental system, the stretch direction is set to be 0^o. Thus, the long axis of a parallel wound is 0^o and the long axis of a perpendicular wound is 90^o. As in the forthcoming discussion below, cells in both wound directionalities tend to align perpendicular with the stretch direction (i.e., the long axis of stretched cells tend to be 90^o). Therefore, stretched cells align perpendicular to the parallel wound, and may cover the parallel wound more quickly (compare Figure 3.1D and Figure 3.2D and refer to Figure 3.3B).

3.2 Cyclic Stretch Induces Distinct Morphological Changes in ECs Subjected to Different Wound Directionalities

EC morphology features were investigated in a cell migration assay under 20% elongational cyclic stretch at 1 Hz frequency for a period of 3 h as described above. Wounds with long axis perpendicular and parallel to the stretch direction were created in

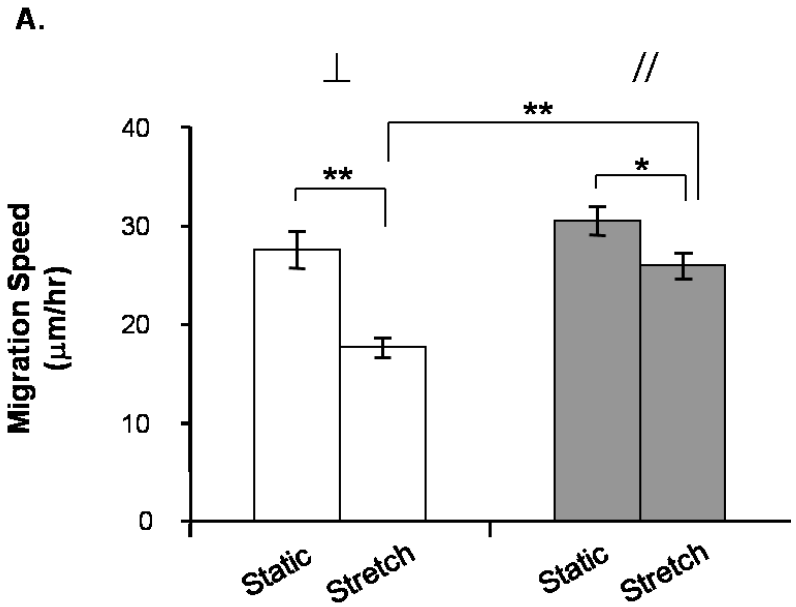

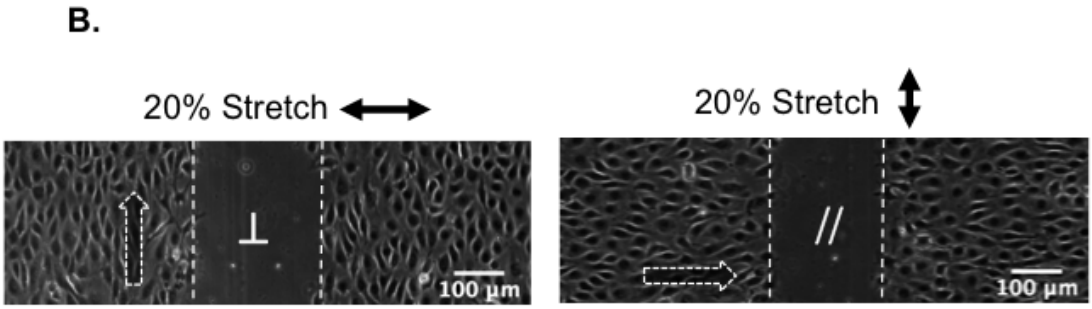

With respect to stretch direction (0°)	⊥ wound	// wound
Long axis of wound	90°	0°
Long axis of cells at and near wound	90°	90°
Anticipated speed	Slower	Faster

Figure 3.3 Cyclic stretch decreased the migration speed of endothelial cells in both wound directionalities. **(A)** White bars: perpendicular (⊥) wounds. Gray bars: parallel (//) wounds. *: p <0.05. **: p <0.025. **(B)** Representative phase contrast images of stretched samples, as well as the orientation of wounds/cells, at the end of the 3 h-experimentation period. In order to cover the denuded area quickly, the cells should align perpendicularly to the area they are moving into. Because cells in the // wound samples align perpendicularly to the wound, they move faster than cells in the ⊥ wound samples, where cells align parallel to the wound.

cell monolayers and ECs were exposed to stretch or kept at static controls. Phase contrast micrographs were recorded using a microscope coupled with a CCD camera, and IPLab was used to determine cell sizes (i.e., areas and perimeters), shapes (i.e., ratios of major axis over minor axis), and cell directionality or orientation (i.e., angle distribution) of cyclically stretched ECs and control ECs.

Results showed the area of cells within the denuded regions was significantly greater in both static controls and under cyclic stretch conditions when compared to their counterpart regions (Figure 3.4). This pattern was observed equally in both perpendicular and parallel wounds. These data are consistent with the literature, which has reported that subconfluent ECs (e.g., such as those scattered in a denuded area) have a larger cellular area than ECs in a confluent monolayer (24-26). If this occurs *in vivo*, a larger cellular area can cover more denuded area, thereby preventing the exposure of subendothelial and thrombogenic extracellular matrices and vascular tissue to platelets.

The cellular perimeter within the denuded regions was also greater in both static controls and under cyclic stretch conditions when compared to their counterpart regions (Figure 3.5), and this is consistent with an increase in cellular area as mentioned above. Again, this pattern was observed in perpendicular and parallel and wounded cells. However, the perpendicular wounded cells had a greater perimeter than parallel wounded cells, suggesting that stretched cells in the wound area were more slender (i.e., hence had a larger long-over-short-axis ratio) in a perpendicular wound than a parallel one. This is consistent with the reported findings below (see Figure 3.6).

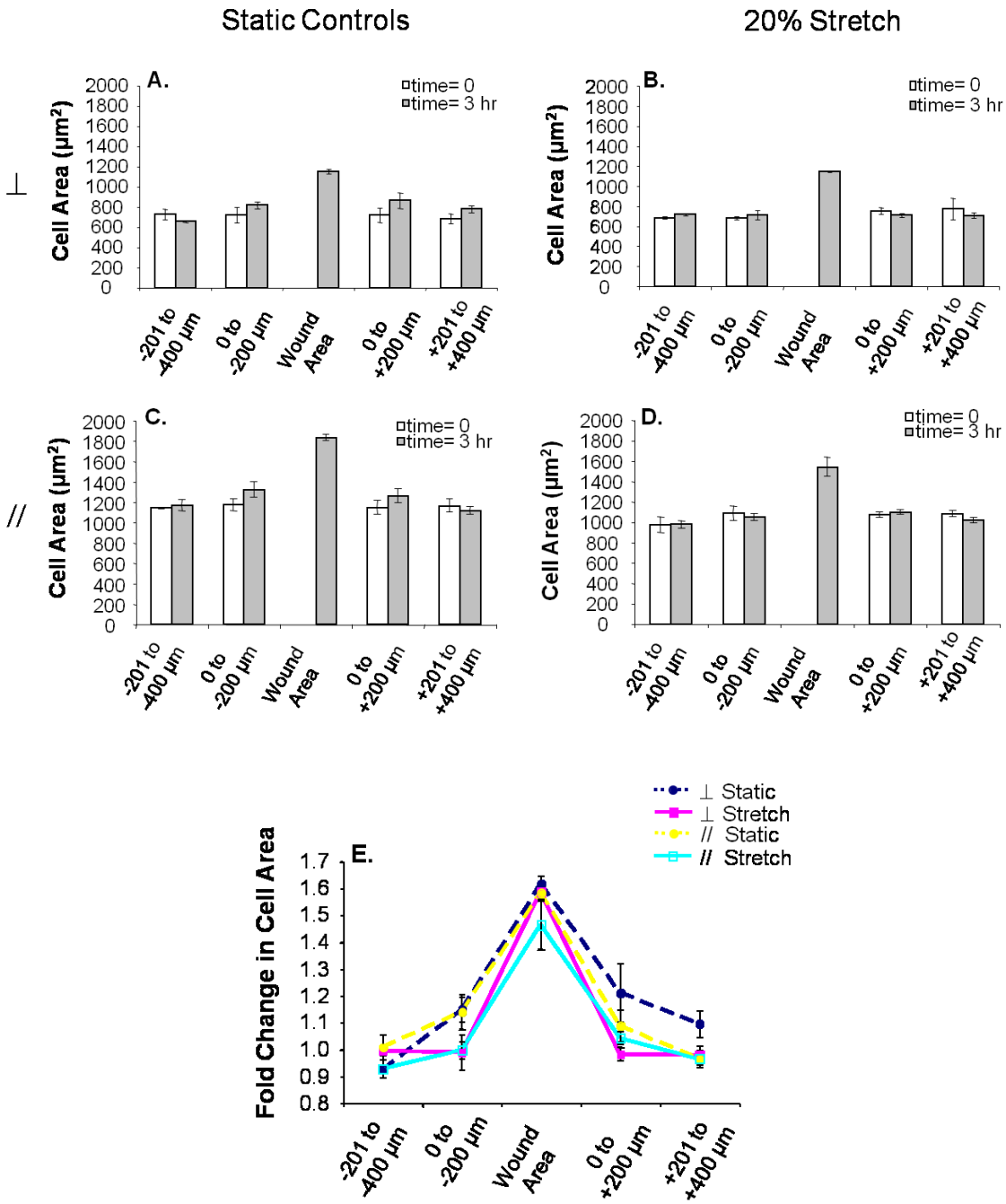

Figure 3.4. Cell area in a wound healing model. The area of cells in five different zones at the beginning (t=0) and end (t=3h) of the experiments was analyzed for perpendicular wounds (**(A)** static controls; **(B)** 20% stretch) and parallel wounds (**(C)** static controls; **(D)** 20% stretch). **(E)** Fold change in cell area at the beginning and end of the experiments was analyzed. Under all conditions, the cell area was significantly increased in the wound area when compared to the other four zones.

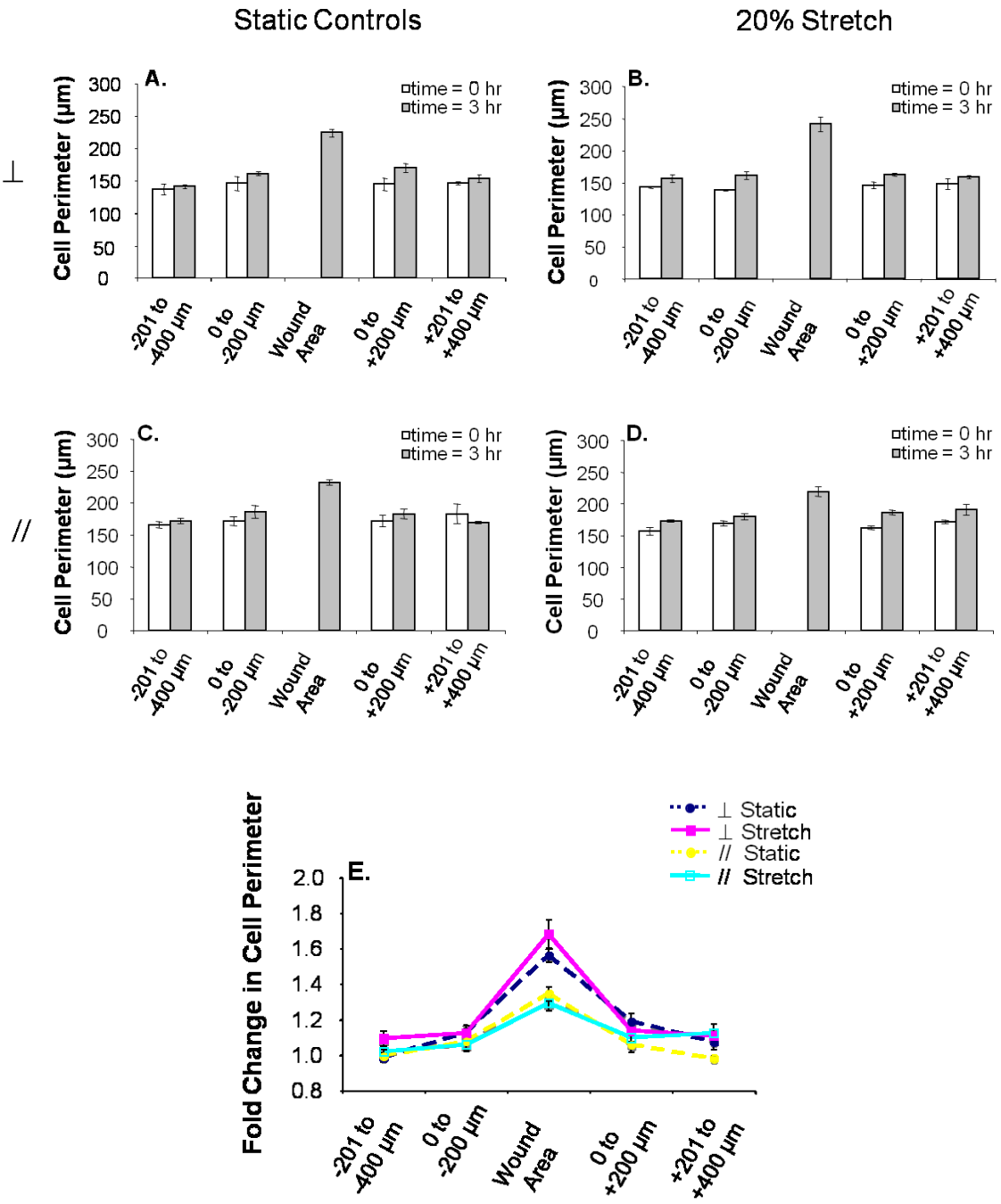

Figure 3.5 Cell perimeter in a wound healing model. The perimeter of cells in five different zones at the beginning (t=0) and end (t=3h) of the experiments was analyzed for perpendicular wounds (**(A)** static controls; **(B)** 20% stretch) and parallel wounds (**(C)** static controls; **(D)** 20% stretch). **(E)** Fold change in cell perimeter at the beginning and end of the experiments was analyzed. Under all conditions, the cell perimeter was significantly increased in the wound area when compared to the other four zones. This observed increase was more pronounced in perpendicular wounds than in parallel wounds.

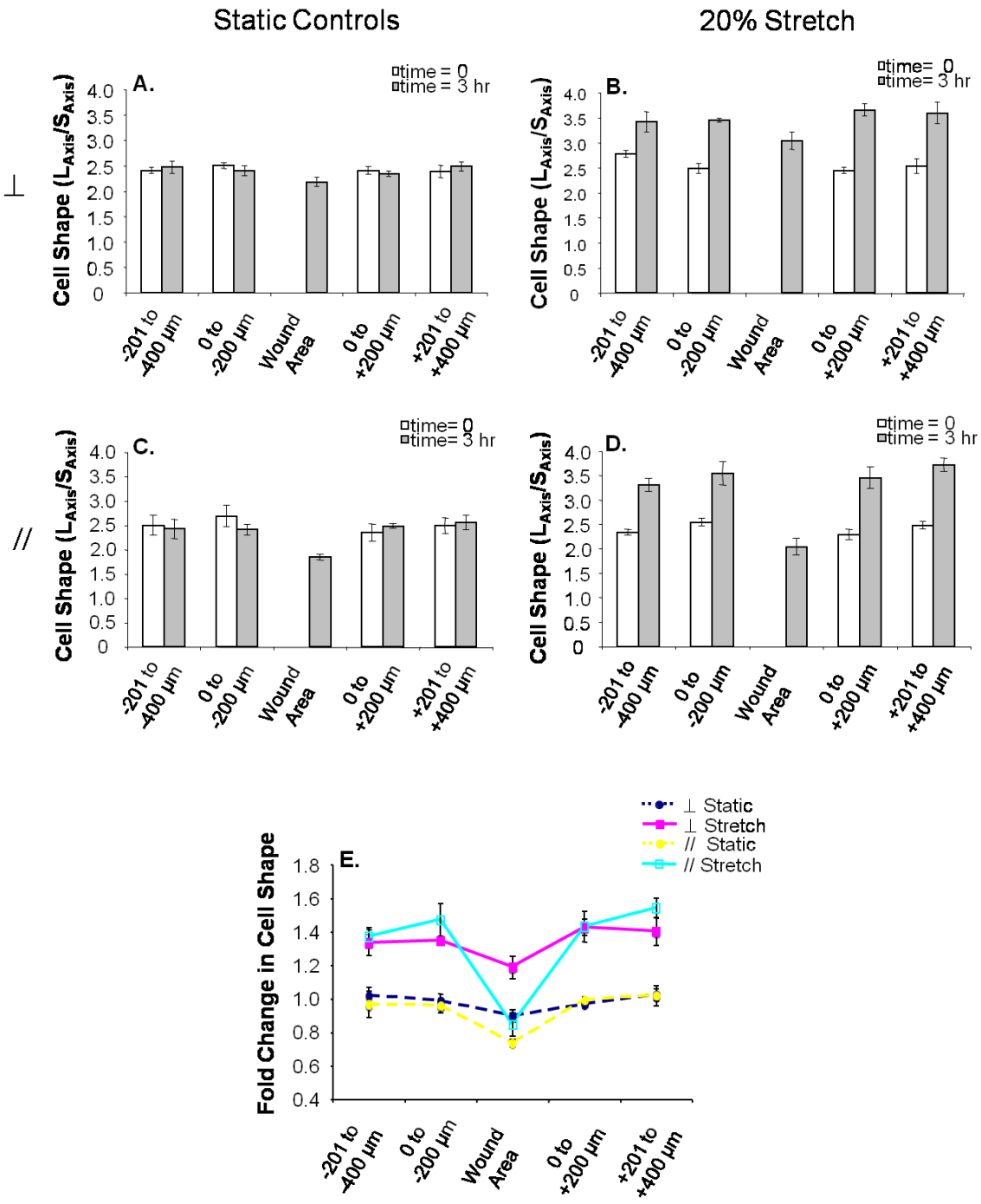

Figure 3.6 Cell shape in a wound healing model. The shape of cells in five different zones at the beginning (t=0) and end (t=3h) of the experiments was analyzed for perpendicular wounds (**(A)** static controls; **(B)** 20% stretch) and parallel wounds (**(C)** static controls; **(D)** 20% stretch). **(E)** Fold change in cell shape at the beginning and end of the experiments was analyzed. The cell shape index was significantly increased by stretch in all the zones of both wound directionalities expect one: the wound area of a parallel wound.

Also observed was that, in both perpendicular and parallel wounds, the cell shape index was significantly increased by stretch in all zones except one (i.e., cells in the denuded area of a parallel wound) (Figure 3.6). As mentioned above, an increased cell shape index under stretch means that cells became more slender under stretch. These slender cells displayed preferential orientation. Cell orientation was measured in terms of cell alignment with respect to the direction of stretch (i.e., being 0°/parallel and 90°/perpendicular to the direction of stretch). Angles were grouped into 3 categories: ≤30°, >30°- ≤60°, and >60° - ≤90° for easier visualization of cell orientation patterns. Stretch significantly increased the percentage of cells in the "$>60° - \leq 90°$" category in all zones except one (i.e., cells in the denuded area of a parallel wound) (Figure 3.7).

Overall, the morphology data suggest that cells away from the denuded area (i.e., cells in a confluent area) became elongated and aligned perpendicular to the stretch direction, regardless the directionality of a nearby denuded area. However, the response of cells in the denuded area (i.e., cells in a subconfluent area) to stretch was affected by the directionality of the denuded area. In a perpendicular wound scenario, the wound's long axis was 90^{o}, which was the same as the directionality that stretched cells tended to develop. In a parallel wound scenario, the wound's long axis was 0^{o}, which may have hindered the development of an elongated cell shape perpendicular to the wound. However, in spite of the relatively lower degree of elongation and preferential alignment in a parallel wound under stretch, these cells can cover the wound more quickly than cells in a perpendicular wound under stretch. This means that a preferred alignment may not be the best for effective migration and swift wound covering. In fact, the angle

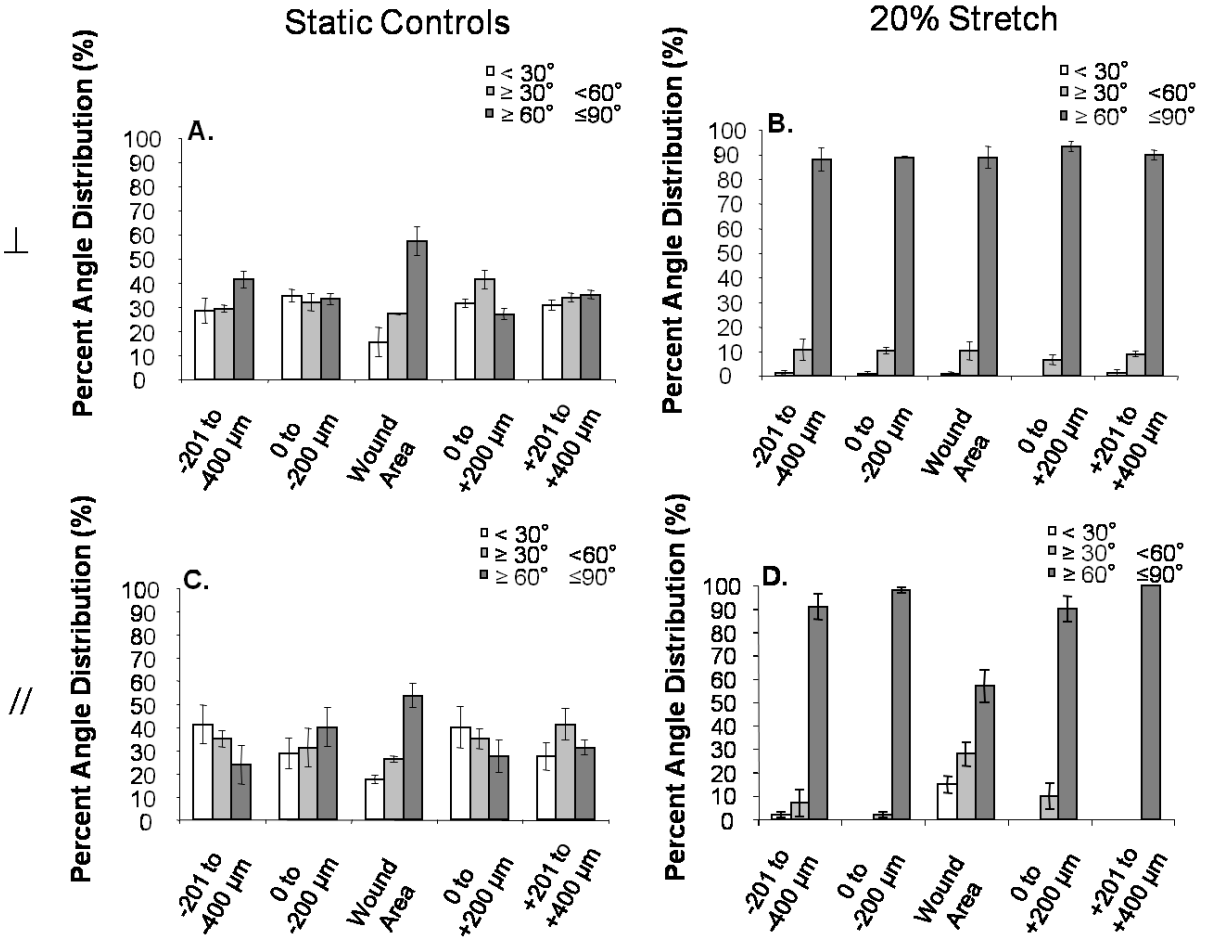

Figure 3.7 Cell orientation in a wound healing model. The orientation of cells in five different zones at the end of the experiments (t=3h) was analyzed for perpendicular wounds (**(A)** static controls; **(B)** 20% stretch) and parallel wounds (**(C)** static controls; **(D)** 20% stretch). The angle distribution at the beginning of the experiments (t=0) was about 33% across the board. Stretch significantly induced perpendicular alignment of cells in all the zones of both wound directionalities. However, this effect is less weak for stretched cells in the wound area of a parallel wound.

distribution of stretched cells in the denuded area of a parallel wound is similar to that in static controls.

The clinical applications of the findings include the consideration of the directionality of surgical incisions. For example, when cutting a large blood vessel wall, such as during arterial bypass surgery, one should create an incision in the circumferential direction and minimize the length of the incision in the axial direction. Additionally, the findings may also explain the focal nature of certain vascular problems such as atherosclerotic lesions and intimal hyperplasic lesions. These lesions tend to develop in regions of increased stretch, and the data suggest that stretch inhibits cell migration.

Next, I investigated the molecular mechanisms underlying the inhibitive effect of stretch on EC migration. Because the inhibitive effect of stretch is stronger in a perpendicular wound scenario, the following experiments were focused on perpendicular wounds only, unless otherwise indicated.

3.3 Cyclic Stretch Induces the Remodeling of Cell-Cell Junctions, Focal Adhesions, and Actin Filaments

Cytoskeletal and transmembrane proteins in ECs under static and stretch conditions were investigated in the migration assay. Specifically, VE-cadherin-mediated cell-cell junctions, vinculin-mediated focal adhesions, and cytoskeletal filaments were examined in this wound healing model. At the end of the experimentation period, EC monolayers were immediately fixed, permeabilized, and stained for cells nuclei, VE-cadherin, an FA protein vinculin, and F-actin filaments. It was found that cyclically

stretched EC samples had fewer and less pronounced numbers of VE-cadherin-stained cell-cell junctions when compared to static controls (Figure 3.8). The total number of vinculin-stained FAs also decreased under cyclic stretch, though FA sizes increased (Figures 3.9). Under cyclic stretch, FAs were localized beneath the center of the cell body while being concentrated in the protruding lamellapodia in static controls and tended to be located at the end of actin filaments (Figures 3.10 and 3.11). Additionally, actin filaments reoriented perpendicularly to the stretch direction similar to the cell body orientation (Figure 3.11) when compared to static controls (Figure 3.10).

In order for cells to move away from a monolayer into a denuded area, there is a need for a transient decrease in the cell-cell junction to give cells the freedom to move. The integrity of the cell-cell junction is usually positively associated with the intensity of fluorescently labeled junctional proteins such as VE-cadherins (22, 33). Our data showed a decreased intensity of VE-cadherin-mediate cell-cell junction under stretch. Thus, the inhibitive effect of stretch on EC migration may not be a result of the lack of cell-cell junction breakdown.

An important requirement of cell migration is the dynamics of FA assembly and disassembly. In cell migration, new FAs form in the moving front and pre-existing FAs in the trailing tail disassemble (2, 6, 16). FAs usually end at the tip of actin filaments, which generate contractile forces needed to propel movement in a migratory cell (13). Large FAs usually support adhesion and are not effective for migration (2). As shown in Figures 3.10 and 3.11, vinculin-stained FAs overlap with actin filaments in both static and stretched cells. In static controls, most of the FAs were located at the cell edge,

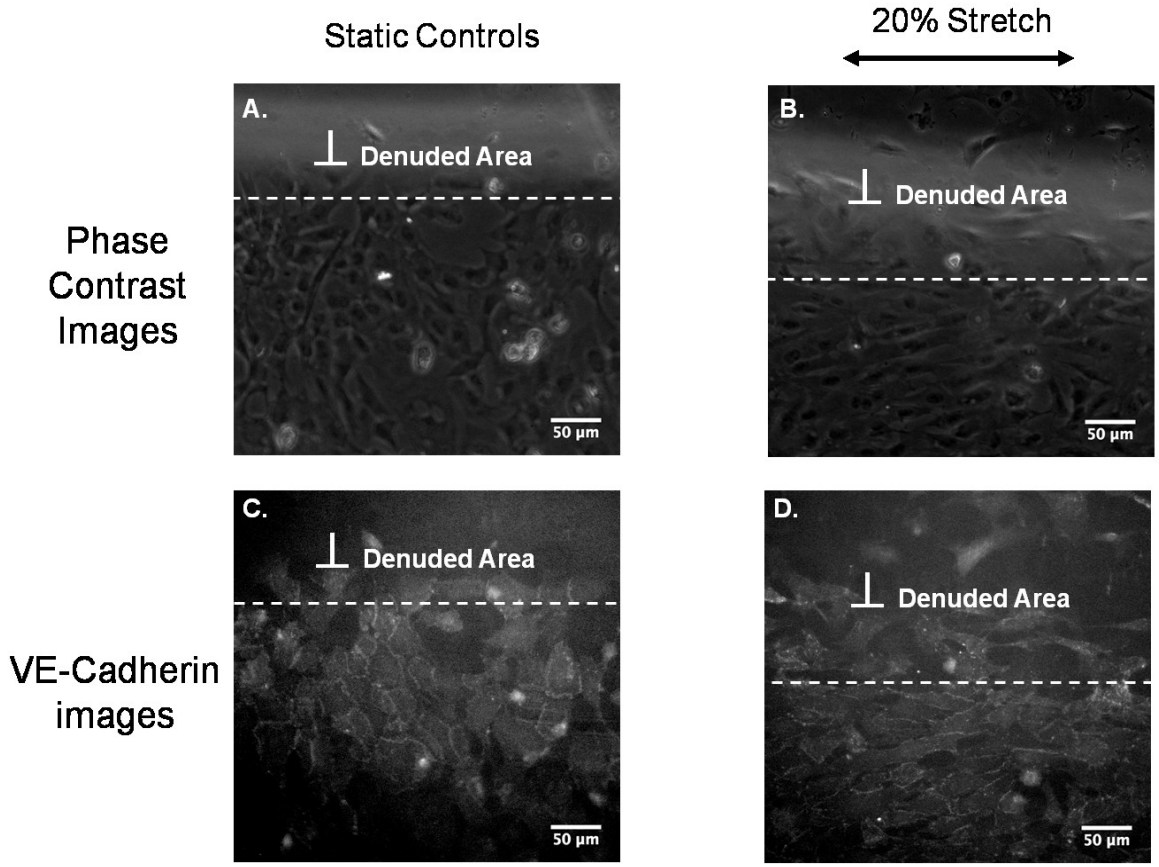

Figure 3.8 Representative microscopic images of vascular endothelial (VE)-cadherin staining in perpendicular (⊥) wound healing. (A) and **(C)** are phase contrast and fluorescent images of a static control sample, respectively. **(B)** and **(D**) are phase contrast and fluorescent images of a 20% stretch sample, respectively. Dashed line indicates the boundary of the wound area at the beginning of the experiment. The images were acquired 3 h later. Double headed arrow indicates stretch direction.

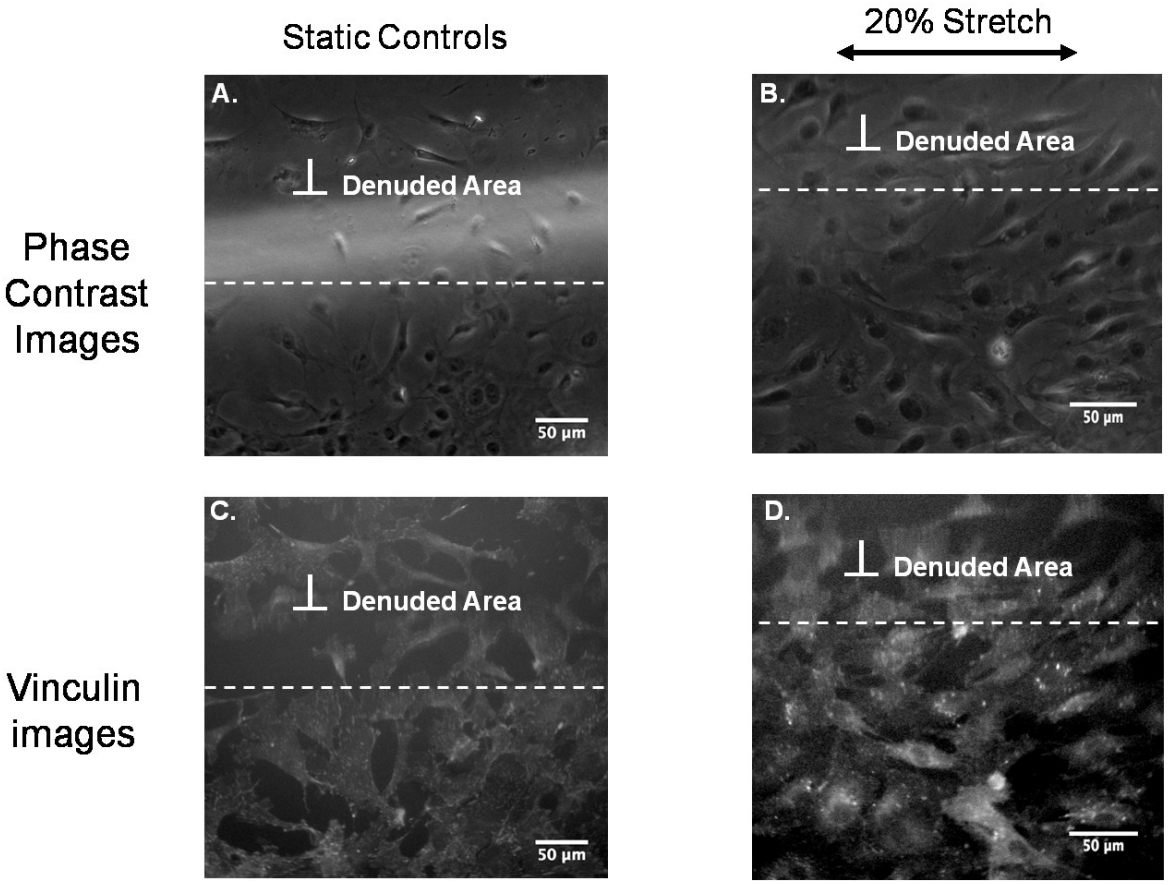

Figure 3.9. Representative microscopic images of vinculin staining in perpendicular (⊥) wound healing. (A) and **(C)** are phase contrast and fluorescent images of a static control sample, respectively. **(B)** and **(D)** are phase contrast and fluorescent images of a 20% stretch sample, respectively. Dashed line indicates the boundary of the wound area at the beginning of the experiment. The images were acquired 3 h later. Double headed arrow indicates stretch direction.

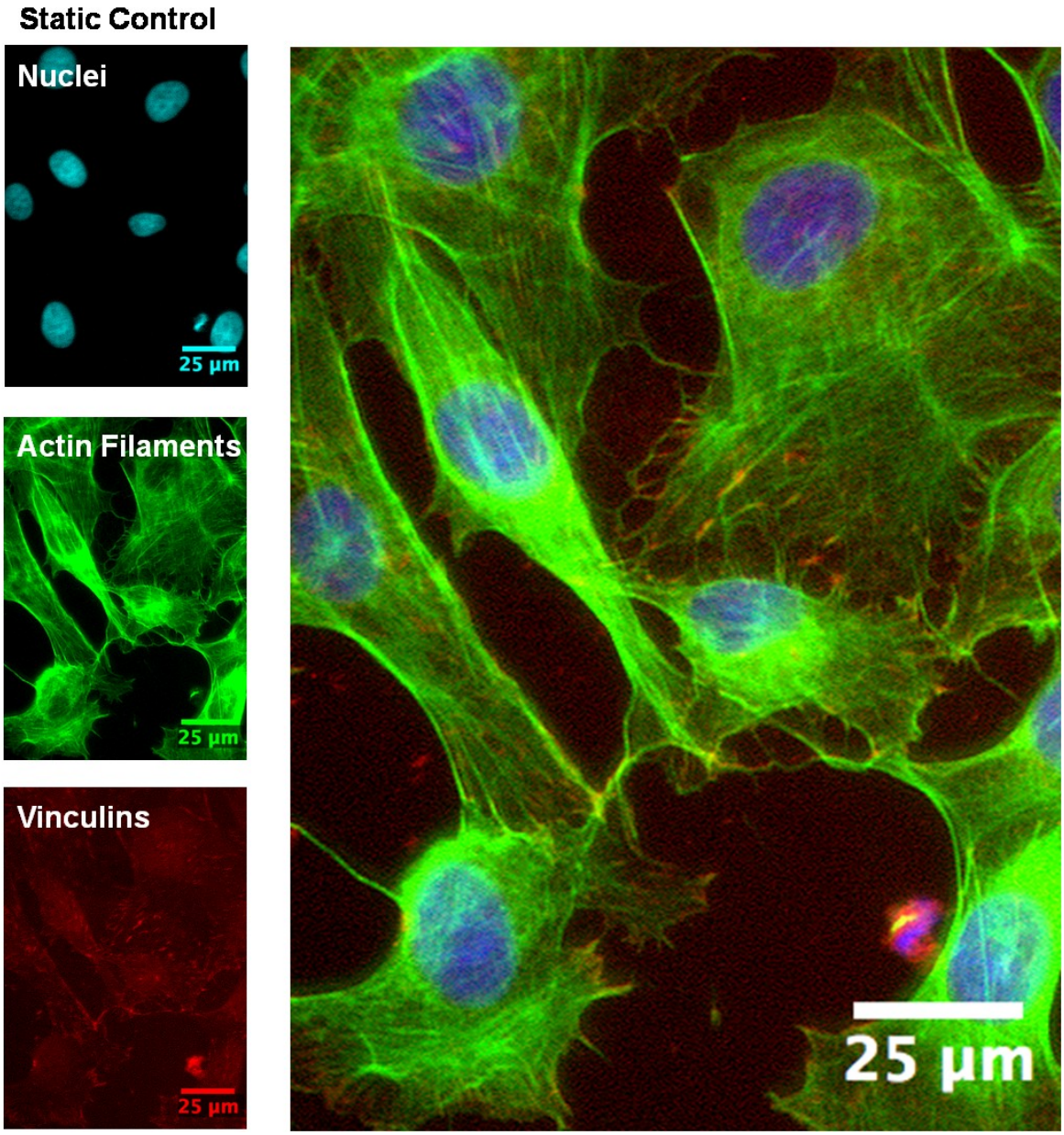

Figure 3.10. Representative microscopic images of fluorescent staining of a static control sample in perpendicular (⊥) wound healing (t=3 h).

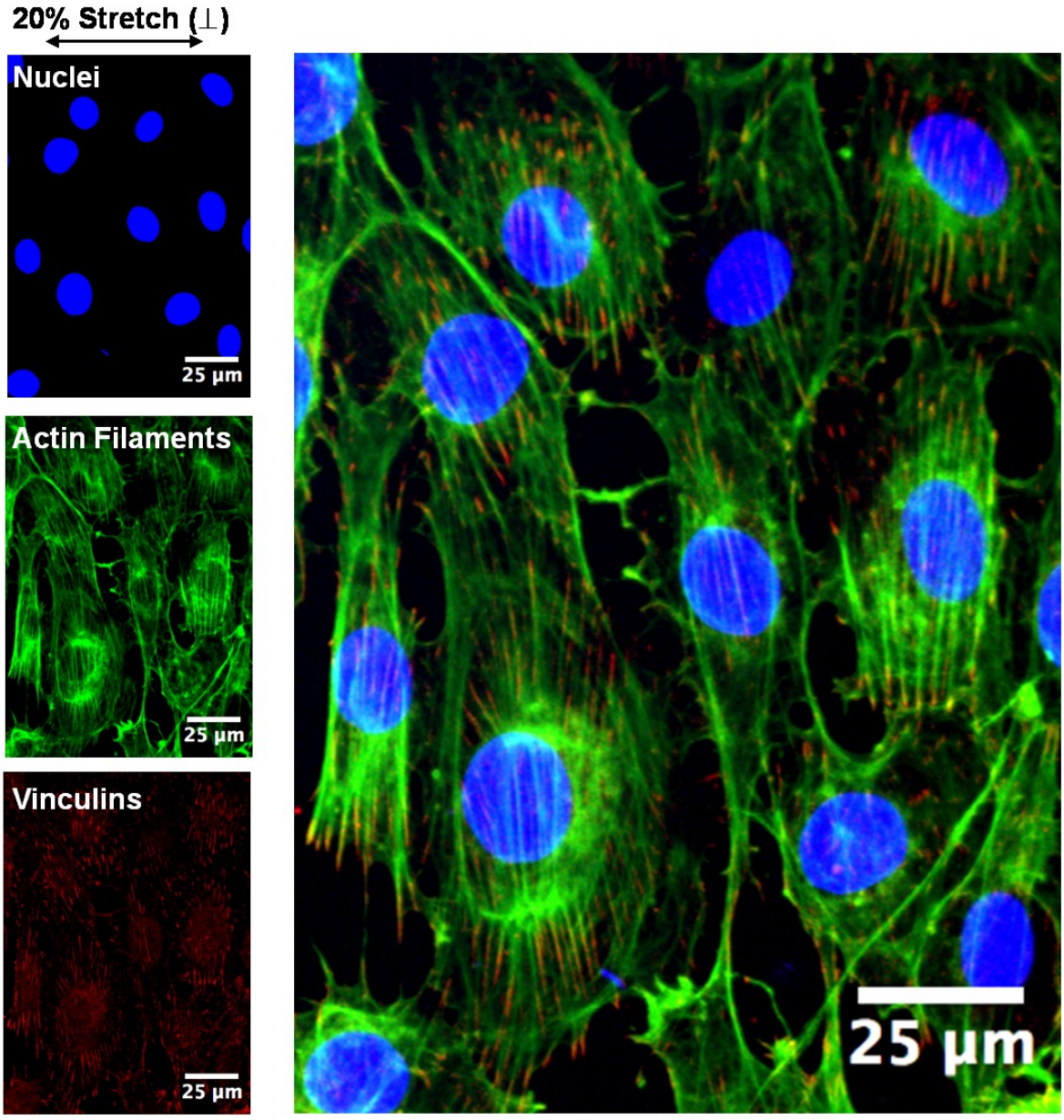

Figure 3.11 Representative microscopic images of fluorescent staining of a 20% stretch sample in perpendicular (⊥) wound healing. Double headed arrow indicates stretch direction. (t=3 h).

while large FAs under the cell body can be found in stretch samples. Therefore, it is possible that under cyclic stretch cells, bigger FAs developed to strengthen adhesion to the underlying substrate, but such a response would hinder cell migration.

3.4 Cyclic Stretch Decreases the Amount of ETS-1 Transcription Factor in the Nuclei

The model included data for the local amounts of ETS-1 transcription factor. Static and stretched cell monolayers were fixed, permeabilized, and stained for ETS-1 at the end of each experiment. ETS-1 amount and specific localization (i.e., cytosol and nucleus) were quantified. ETS-1 is an important transcription factor regulating wound healing as activated ETS-1 translocates from the cytosol to the nuclei (20, 44, 46). In static controls, the amount of ETS-1 in the nuclei was significantly higher than in the cytosol, and the amount was higher in the wound area than far away from the wound. This finding is consistent with the literature reporting an increased ETS-1 in wounded ECs than in quiescent EC monolayers. The amount of ETS-1 in the cytosol was the same in the static controls and stretched samples in all zones. However, stretch significantly decreased the amount of ETS-1 in the nuclei when compared to static controls (Figure 3.12). Further, the amount of nuclear ETS-1 was the same in stretched cells in all zones. Therefore, it is possible that the inhibitive effect of stretch on EC migration is via inhibiting ETS-1 production.

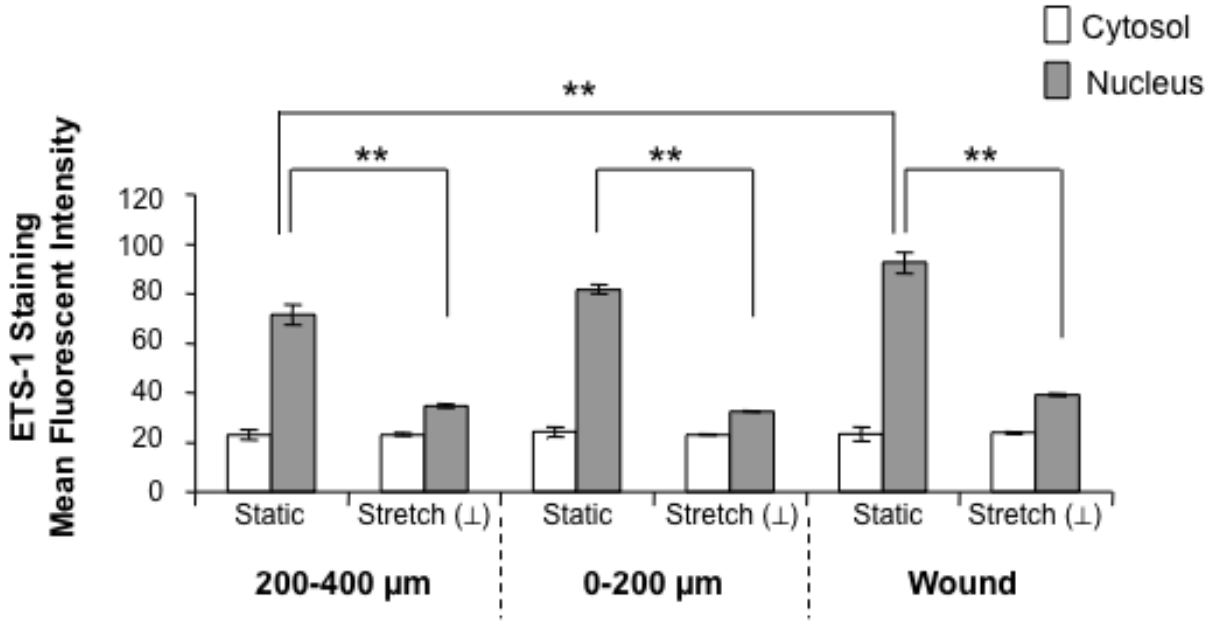

Figure 3.12 Cyclic stretch decreased the amount of ETS-1 transcription factor in the nuclei. The amount of ETS-1 in the cytosol (i.e., white bars) was similar in static controls and 20% stretch samples and in all different zones 3 h after wounds were created. However, static controls had more ETS-1 in the nuclei than in stretched samples. Additionally, in static controls, the nuclei of cells in the wound area had more ETS-1 than those far away from the wound **$p<0.025$.

3.5 Stretch Increased ROS but EC Migration Speed Did Not Recover upon Removal of Intracellular ROS

An excess of ROS or its inadequate metabolism can induce oxidative stress, though low physiological ROS levels can also be critical in cell signaling. Excess ROS has been shown to impair EC migration (4). The literature has also indicated that stretch induces ROS generation. The current experiments investigated whether the inhibitive effect of stretch on EC migration is mediated by ROS. It was initially confirmed that ROS, indeed, is up-regulated in the experimental system. At the end of experiments, injured EC monolayers were stained for intracellular ROS using CM-H_2DCFDA and then observed under fluorescent microscopy. Fluorescent intensities of cells were determined using IPLab as described previously. Data indicated cyclic stretch increased the intensity of ROS by twofold when compared to static controls. Next, I tested my hypothesis using ROS inhibitors.

ECs were exposed to two common chemical regulators of intracellular ROS (i.e., NAC and DPI) and investigated under cyclic stretch in a cell migration assay. After a 1 h incubation period with NAC or DPI, wounded cell monolayers were exposed to 20% membrane elongation strain at 1 Hz for 3 h or kept at static controls. Phase contrast images of wounds were recorded with a microscope coupled with a CCD camera and used to determine the change in wound sizes and subsequently to calculate EC migration speed via imaging software (IPLab) as described above.

NAC is a nonspecific ROS scavenger. NAC treatment in static ECs decreased EC migration speed, and ECs treated with NAC and subjected to cyclic stretch conditions significantly decreased their speed with respect to stretched ECs with no NAC treatment.

The decrease in migration speed in stretched NAC-treated cells was more pronounced than in stretched, untreated cells and when compared to static, untreated cells (Figure 3.13).

DPI, a potent ROS-generating enzyme inhibitor, was selected to treat ECs upon exposure to uniaxial cyclic stretch. It was found that the DPI inhibitor had similar effects on cell migration as the NAC ROS scavenger (Figure 3.14). Therefore, while stretch indeed increased ROS generation, ROS may not be involved in mediating the inhibitive effect of stretch on cell migration.

3.6 Additive Effects of Hyperplasia and Stretch on EC Migration and Morphology

3.6.1 Additive Effects of Hyperplasia and Stretch on Inhibiting EC Migration and the Role of ROS

It has been well-established that patients with both hypertension and hyperglycemia conditions (i.e., as in the case of diabetic patients) suffer from a higher risk of cardiovascular disease than others with chronic disease conditions. The beneficial effect of antioxidant-based therapy in these patients has been controversial, which led to the hypothesis that hypertension (approximated here by stretch) and hyperglycemia (approximated here by high glucose concentration) have additive effects upon inhibiting cell migration through both similar and different pathways.

EC migration was investigated in a "wound healing" scenario similar to that previously described above. The difference was the use of normal glucose concentration

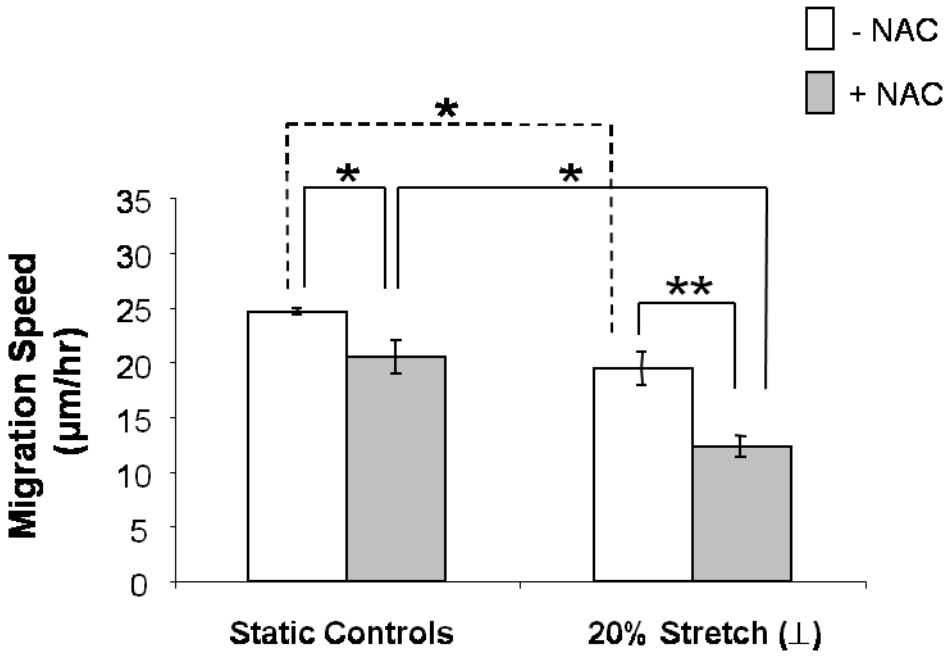

Figure 3.13 Intracellular ROS scavenger NAC did not recover migration speed under stretch. *: p <0.05. **: p <0.025.

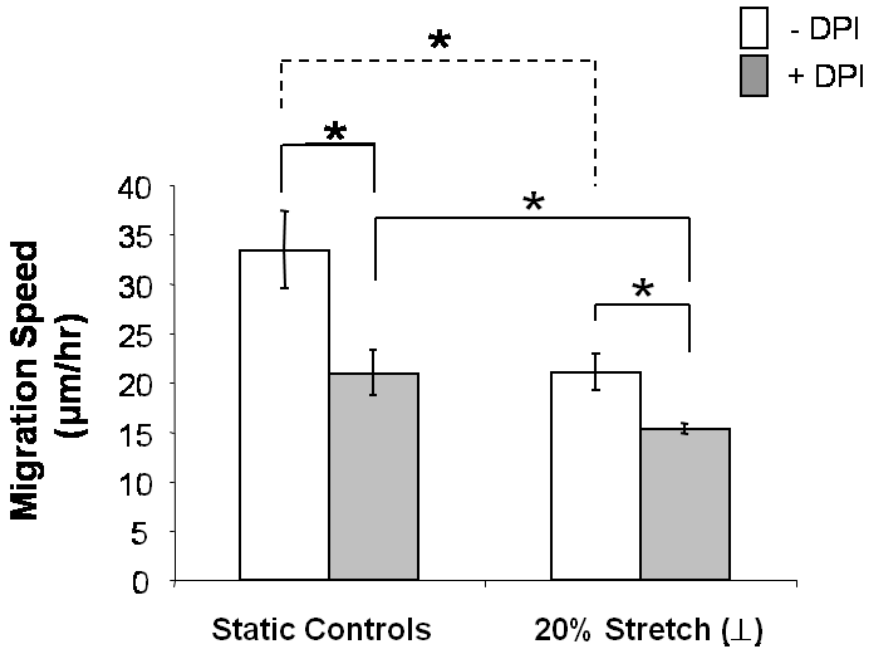

Figure 3.14 ROS generating enzyme inhibitor DPI did not recover migration speed under stretch. *: p <0.05.

(as in the previous sections) and high glucose concentration at the same experimental conditions (i.e., static vs. 20% stretch and 1 Hz). It was found that static hyperglycemic conditions caused a decrease in migration speed when compared to static normal glycemic conditions, and this decrease apparently can be prevented by NAC (Figure 3.15). As NAC can block the inhibitive effect of hyperglycemia but not that of stretch, the data suggest that stretch and hyperglycemia inhibit cell migration through somewhat different mechanisms. In terms of clinical applications, the data would also suggest that antioxidant-based therapy may not be sufficient because it does not prevent the stretch effect.

Cyclic stretch caused a further decrease in the migration speed of ECs under hyperglycemic conditions, when compared to static hyperglycemic controls (Figures 3.16 and 3.17). This additive effect of hyperglycemia and cyclic stretch caused an overall large decrease in the migration speed of ECs, similar to pathologic observations relative to prevailing conditions of atherosclerosis and other vascular complications in diabetic patients.

Hyperglycemic ECs were exposed to two common chemical regulators of intracellular ROS (i.e., NAC and DIP) and were investigated under cyclic stretch in a cell migration assay as described in Section 3.5. Data indicated NAC treatment in static/HG ECs increased their migration speed when compared to untreated static/HG ECs. However, hyperglycemic ECs treated with NAC and subjected to cyclic stretch conditions were shown to be not significantly different with respect to stretched and hyperglycemic ECs with no NAC treatment (Figure 3.16). In contrast, for static/HG conditions, cell migration speed did not change with the treatment of DPI compared to

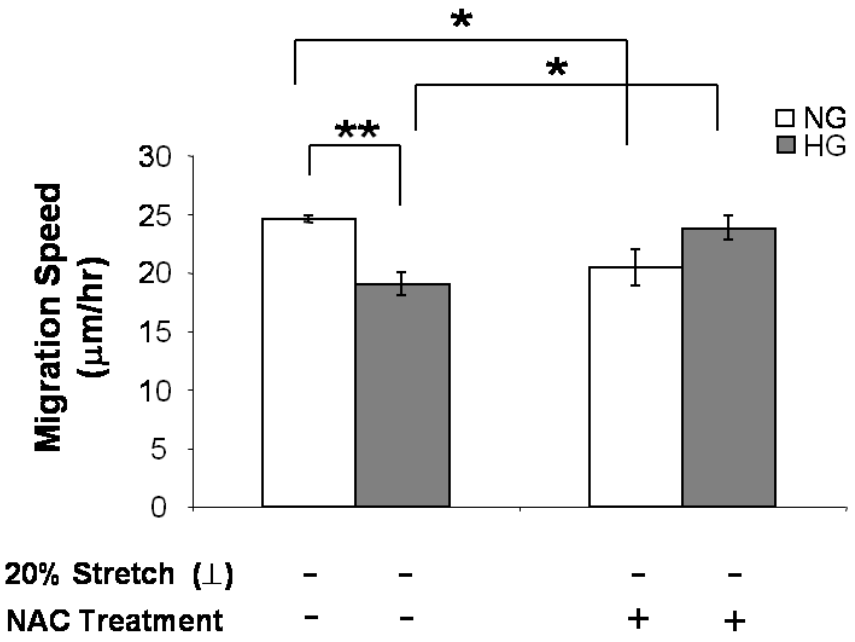

Figure 3.15 Intracellular ROS scavenger NAC recovered migration speed under hyperglycemia. High glucose (HG) decreased migration speed in static controls when compared to normal glucose (NG). This inhibitory effect was blocked by NAC. *: p <0.05. **: p <0.025.

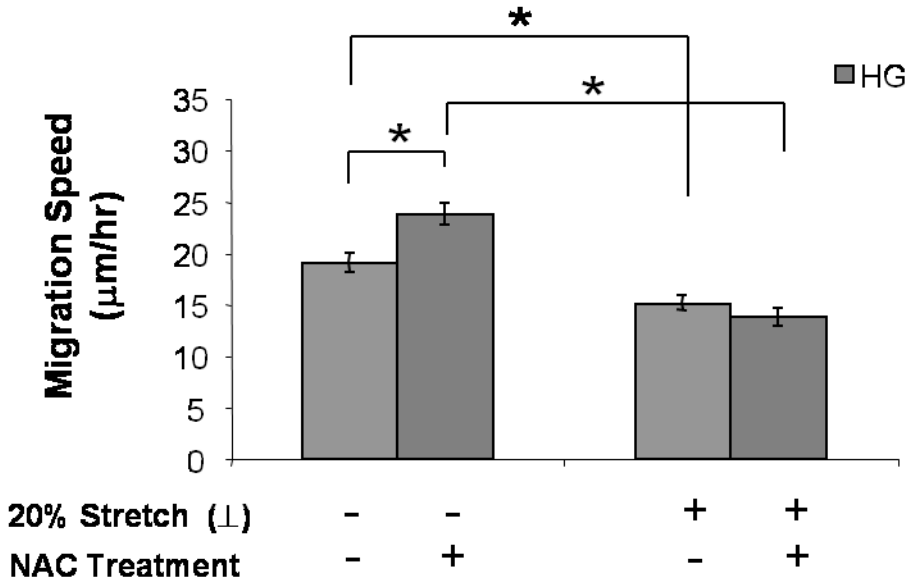

Figure 3.16 Intracellular ROS scavenger NAC did not recover migration speed under stretch and hyperglycemia. Stretch decreased the migration speed of high glucose (HG)-treated cells. However, this inhibitory effect was not blocked by NAC. *: p <0.05.

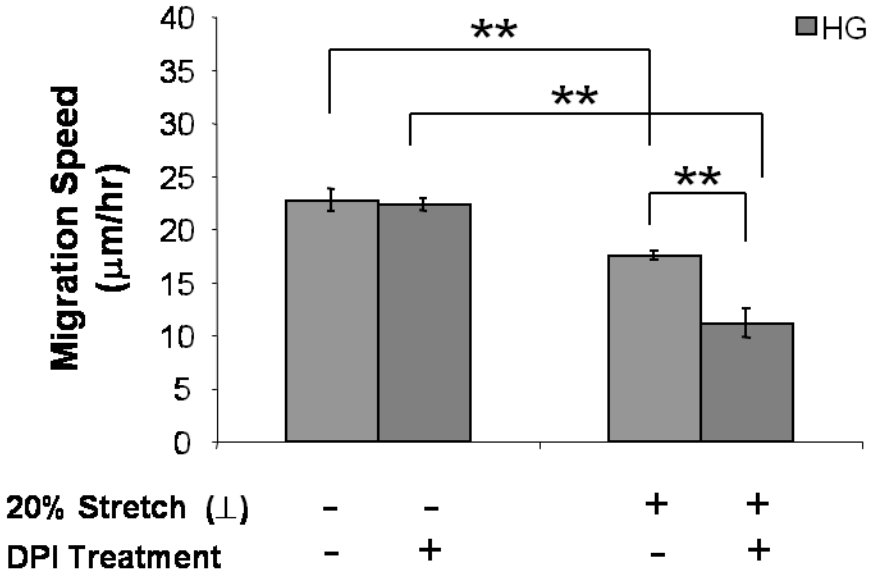

Figure 3.17 ROS-generating enzyme inhibitor DPI did not recover migration speed under stretch and hyperglycemia. Stretch decreased the migration speed of high glucose (HG)-treated cells. However, this inhibitory effect was not blocked by DPI. The migration speed of HG-treated and stretched cells was further decreased by DPI. **: p <0.05.

static/HG untreated ECs. Further, DPI-treated hyperglycemic ECs under cyclic stretch conditions significantly decreased their ability to migrate when compared to untreated hyperglycemic ECs under stretch (Figure 3.17). The decrease in migration speed in stretched DPI-treated hyperglycemic cells was more pronounced than in untreated cells.

3.6.2 Cyclic Stretch and Hyperglycemia Induced Distinct Morphological Changes in ECs

Morphological features of ECs cultured in high glucose conditions were investigated in a cell migration assay under 20% uniaxial cyclic stretch at 1 Hz for 3 h as described in Section 3.2. Results showed the area of HG-treated cells within the denuded regions was significantly greater in both static controls and under cyclic stretch conditions when compared to their counterpart regions (Figure 3.18). However, such an increase was significantly smaller when compared to NG-treated cells. The perimeter of HG-treated cells within the denuded regions was also greater in both static controls and under cyclic stretch conditions when compared to their counterpart regions (Figure 3.19), and this is consistent with an increase in cell area, as mentioned above. However, again, such an increase was significantly smaller when compared to NG-treated cells.

The cell shape index (Figure 3.20) and orientation (Figure 3.21), however, showed that HG-treated cells became elongated and preferentially aligned perpendicular to the stretch direction, similar to NG-treated cells. Thus, the ability for cells to elongate and align with stretch direction was not hindered by HG treatment.

Cumulatively, the data suggest that the decrease in cell area by HG may contribute to the decrease in migration speed and hence the wound healing rate in

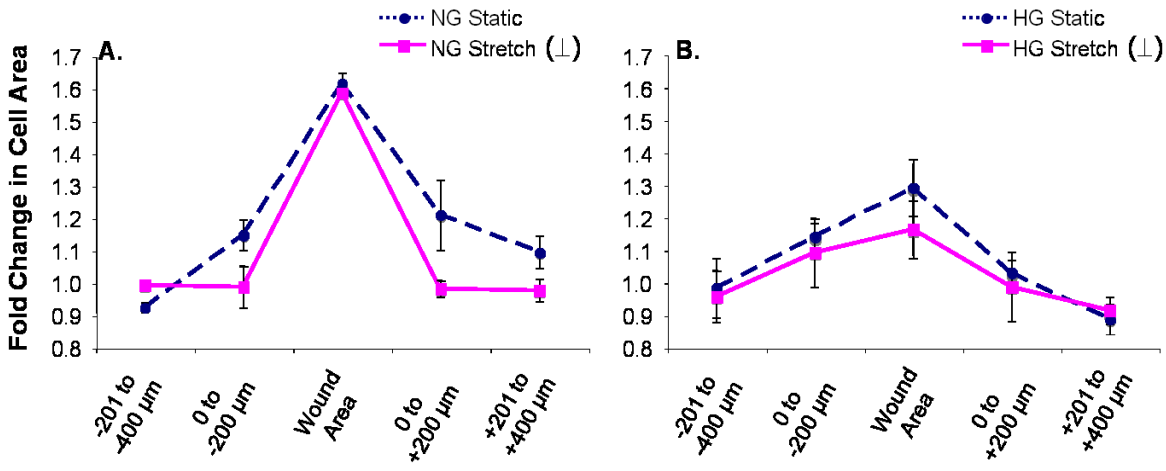

Figure 3.18 Cell area in a hyperglycemia and wound healing model. The area of cells in five different zones was analyzed for perpendicular wounds under **(A)** normal glucose (NG) and **(B)** high glucose (HG) conditions. Fold change in cell area at the beginning and end of the experiments was analyzed. Under all conditions, the cell area was increased in the wound area. Such an increase was not affected by stretch, and was smaller in HG-treated cells.

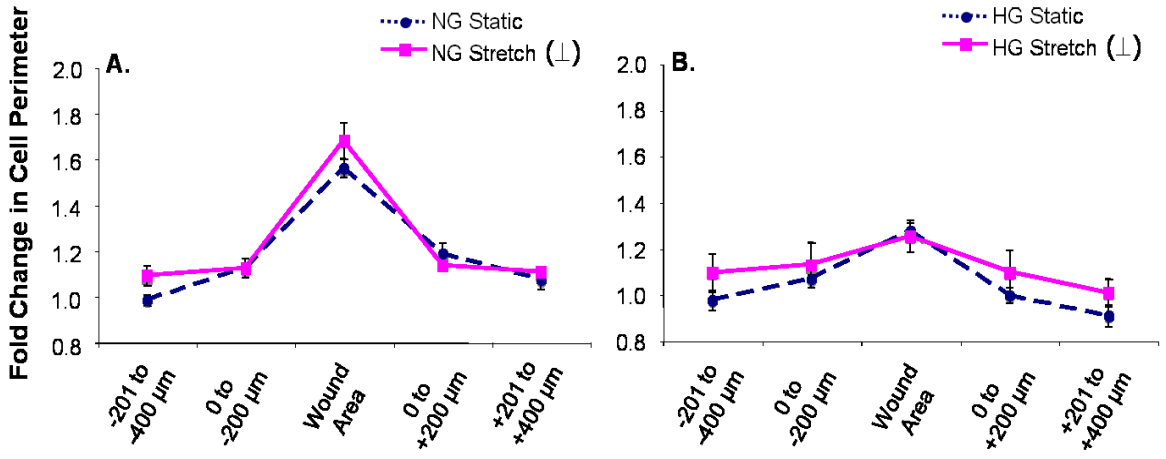

Figure 3.19 Cell perimeter in a hyperglycemia and wound healing model. The perimeter of cells in five different zones was analyzed for perpendicular wounds under **(A)** normal glucose (NG) and **(B)** high glucose (HG) conditions. Fold change in cell perimeter at the beginning and end of the experiments was analyzed. Under all conditions, the perimeter was increased in the wound area. Such an increase was not affected by stretch, but was smaller in HG-treated cells.

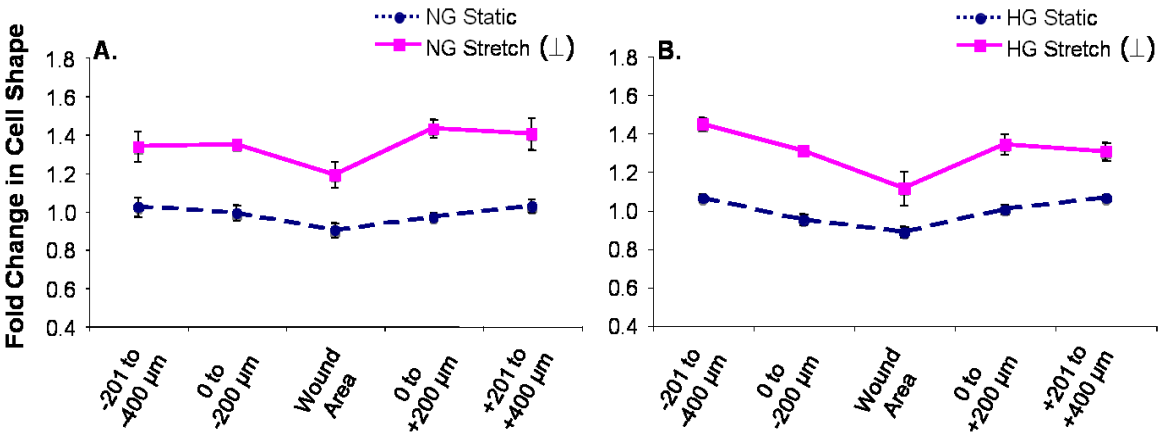

Figure 3.20 Cell shape in a hyperglycemia and wound healing model. The shape of cells in five different zones was analyzed for perpendicular wounds under **(A)** normal glucose (NG) and **(B)** high glucose (HG) conditions. Fold change in the cell shape index at the beginning and end of the experiments was analyzed. Under all conditions, the shape index was increased by stretch. Such an increase was not affected by hyperglycemia.

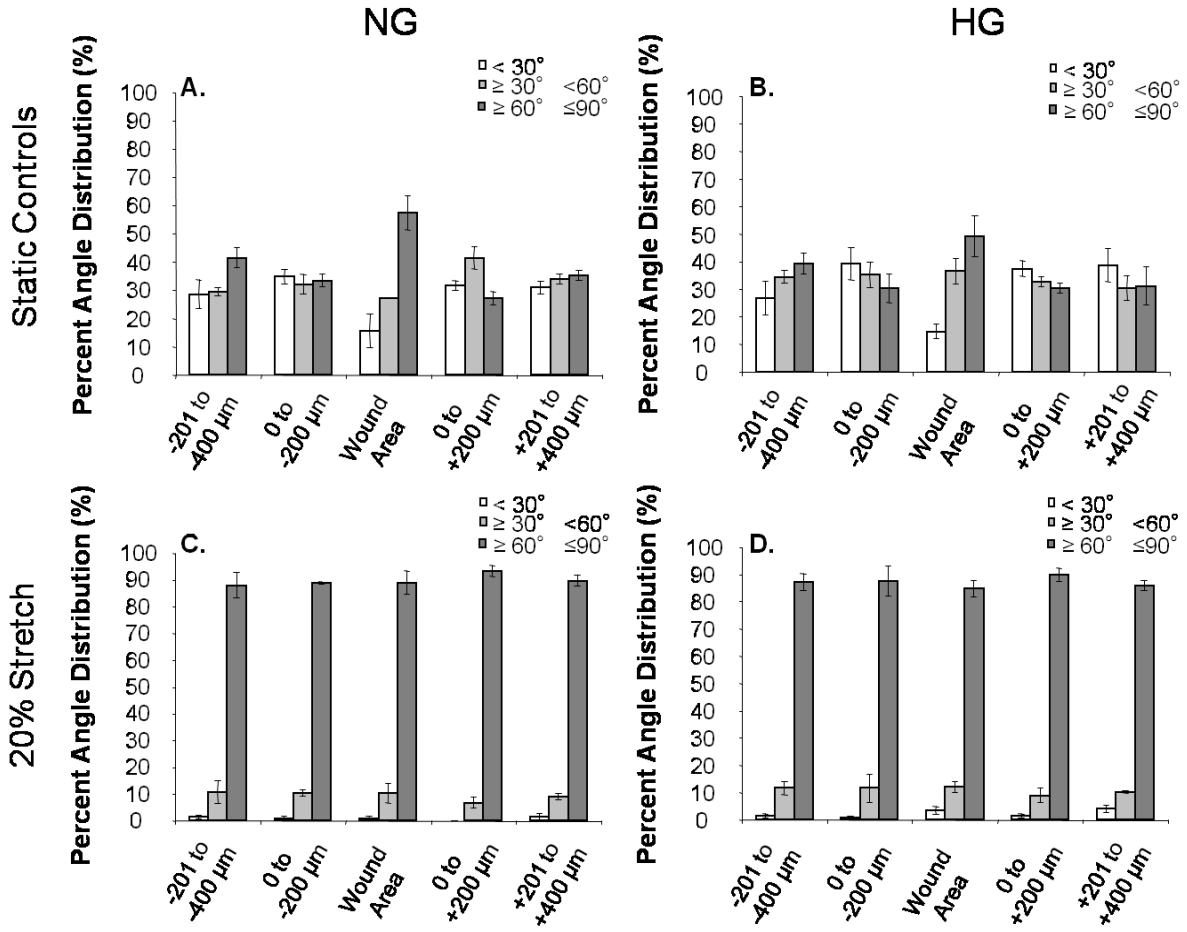

Figure 3.21 Cell orientation in a hyperglycemia and wound healing model. The orientation of cells in five different zones at the end of the experiments (t=3h) was analyzed for perpendicular wounds under normal glucose (NG) conditions (**(A)** static controls; **(C)** 20% stretch) and high glucose (HG) conditions (**(B)** static controls; **(D)** 20% stretch). The angle distribution at the beginning of the experiments (t=0) was about 33% across the board. Stretch induced perpendicular alignment of cells in both NG and HG conditions.

hyperglycemic conditions. When this occurs *in vivo*, HG-treated ECs will not be able to migrate into and cover a denuded area effectively, thereby increasing the exposure time of subendothelial and thrombogenic extracellular matrices and vascular tissue to platelets. This is consistent with clinical findings that patients, who suffer both hypertension and hyperglycemia, have a higher propensity to vascular damage and higher risks for cardiovascular disorders.

3.7 Fluid Oscillation Controls

Some studies have shown that devices applying cyclic deformation to cells also produce some oscillatory fluid motion due to the "nonslip" boundary conditions at the wall. It is conceivable that motion control stretch (i.e., which generates oscillatory fluid shear stress only) and cyclic stretch (i.e., which generates both oscillatory fluid shear stress and cellular deformation) likely have significantly different effects on the ECs.

Fluid oscillation experiments were conducted to rule out any fluid shear stress effects on ECs created by media agitation with the cyclic of the moving shaft in the model system. In these “motion controls,” the polycarbonate templates were not fixed at the stationary end and were attached only to the shaft in the moving end, thus resulting in free movement of the entire polycarbonate template. The silicone membranes in motion control samples were displaced without being stretched for an identical distance and frequency as in the case with their stretched counterparts. Cell migration speeds in the static and motion controls samples for both normal and hyperglycemic conditions were not statistically different from each other (Figure 3.22). Therefore, it could be concluded

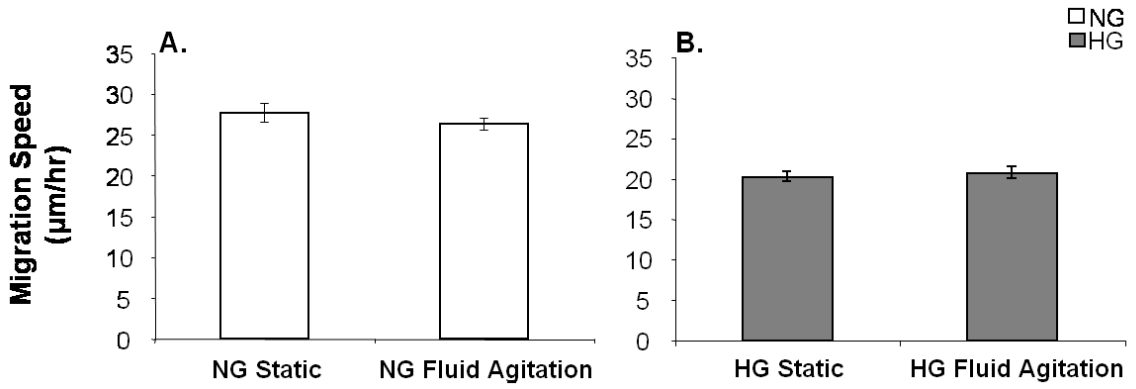

Figure 3.22 Fluid agitation alone did not affect migration speed. The migration speeds of normal glucose (NG)-treated and high glucose (HG)-treated cells are shown in **(A)** and **(B)**, respectively. Static controls and motion controls (i.e., fluid agitation only) had similar migration speeds.

that the stretch effects reported above were not merely the effect of oscillatory shear stress.

CHAPTER 4

CONCLUSION AND FUTURE DIRECTIONS

4.1 Conclusion

Herein examined was the decrease of migration speed in BAECs in a wound healing model under uniaxial cyclic stretch using a custom-designed cell stretching device. The results showed that cyclic stretch decreased the EC migration speed in wounds with both long axes perpendicular and parallel to the stretch direction. This decrease in migration speed was significantly greater in ECs within perpendicular wounds than in parallel wounds, a finding that explains the potential importance of selective surgical incision directionalities to promote faster wound healing.

In order to understand the possible mechanisms leading to the decrease of migration under cyclic stretch, the effects of uniaxial cyclic stretch on EC morphology, cytoskeletal remodeling (VE-cadherin-mediated cell-cell junction, vinculin-mediated focal adhesions, actin filaments), ETS-1, and ROS also were investigated. It was found that stretch did not affect the area or perimeter of cells, but it promoted the elongation and preferential alignment of cells perpendicular to the stretch direction. For subconfluent cells (i.e., such as those in a wound area), this effect was affected by the shape (or, spatial boundary condition) of the denuded area. It also was found that stretch

decreased VE-cadherin-mediated cell-cell junctions and induced the same preferential alignment of actin filaments. Further, stretch changed the focal adhesion dynamics (i.e., more specifically, enhanced focal adhesions for adhesion rather than migration) and decreased the amount of pro-wound healing transcription factor ETS-1. Both mechanisms may explain why EC migration speed and hence, the wound healing rate was decreased by stretch.

As cyclic stretch induced an increase in the amounts of intracellular ROS and as excessive ROS is known to inhibit cell migration, ROS inhibitory studies were merited. Investigating cell migration recovery by using two chemical reagents (e.g., NAC and DPI) to prevent the increase of excessive intracellular ROS, the results showed neither reagent helped speed recovery. This suggests the decrease of migration speed in stretched ECs might not be solely due to the excess of intracellular ROS amounts.

Results from the hyperglycemia wound healing studies showed that hyperglycemia and stretch have additive effects on inhibiting EC migration, but likely through different mechanisms. Hyperglycemia hindered the increase in cell area/perimeter in the wound zone, and the inhibitive effect of hyperglycemia on migration was blocked by NAC. These findings were the opposite of those in stretch experiments with normal glycemia.

In the current study, the two-dimensional cell migration/wound healing assay was validated by incorporating motion control samples in the system, to rule out any effect of the media viscous drag as a result of the cyclic stretch motion. Results indicated fluid shear stress did not affect nor influence the decrease in cell migration speed.

4.2 Future Directions

These findings generate new perspectives on preferential localization of atherosclerosis and possible molecular mechanisms of reduced EC motility under cyclic stretch. Because of the complexity of cellular systems, a great deal of opportunities exists for future investigations. First, all experiments in this study were conducted with arterial cells (i.e., BAECs). However, it is also essential to use cells from other sources for investigating differential effects in vascular healing because it is widely known that ECs from different species and tissue types react differently to stretch.

Second, it remains important to assess EC migration and ETS-1 transcription factor regulation under other strain magnitudes (i.e., 2.5% and 10%). Additionally, other frequencies could be considered beyond the 1 Hz frequency experimented (which mimics the heart's normal pump rate) in the current study. Accelerated and decelerated rates might elicit different effects and fine tune insights about any potential differences in the wound healing process between cardiovascular patients with active and sedentary lifestyles.

Third, besides the cadherins and vinculins employed in this study, there are other cytoskeletal and focal adhesion proteins such as talin, catenin, paxillin, tensin, and others that merit study with regard to their role in any decrease of cell migration speed.

Fourth, the concentrations of the two ROS inhibitors used in this study followed the conventions other studies published in the literature. This might not have been ideal due to the possible interacting effects of stretch plus chemical toxicity that could have exacerbated stress-induced pressures further upon cells. Changes in dosing strategies would add further focus to these observed effects.

Finally, the current studies were performed in a 2-D model ideal to investigate EC migration into a denuded area. However, future studies might evolve into a 3-D model that will broaden and deepen the fundamental understanding of the earliest steps of sprouting angiogenesis. Such models also would help to uncover the complex molecular steps in the cell-cell interactions involving tumor cells and the migration of vascular smooth muscle cells (SMCs) that play an important role in the angiogenic switch, including activating tumor angiogenesis and promoting the maturation of new blood vessels.

REFERENCES

1. **Ascher E, Gade PV, Hingorani A, Puthukkeril S, Kallakuri S, Scheinman M, and Jacob T**. Thiamine reverses hyperglycemia-induced dysfunction in cultured endothelial cells. *Surgery* 130: 851-858, 2001.

2. **Balaban NQ, Schwarz US, Riveline D, Goichberg P, Tzur G, Sabanay I, Mahalu D, Safran S, Bershadsky A, Addadi L, and Geiger B**. Force and focal adhesion assembly: a close relationship studied using elastic micropatterned substrates. *Nature Cell Biology* 3: 466-472, 2001.

3. **Bazzoni G, and Dejana E**. Endothelial cell-to-cell junctions: molecular organization and role in vascular homeostasis. *Physiological Reviews* 84: 869-901, 2004.

4. **Bell L, and Madri JA**. Influence of the angiotensin system on endothelial and smooth muscle cell migration. *The American Journal of Pathology* 137: 7-12, 1990.

5. **Berne RMaMNL**. The cardiovascular system. In: *Physiology*. St. Louis: Mosby, 1998, p. 319-513.

6. **Bershadsky AD, Balaban NQ, and Geiger B**. Adhesion-dependent cell mechanosensitivity. *Annual Review of Cell and Developmental Biology* 19: 677-695, 2003.

7. **Birukov KG**. Cyclic stretch, reactive oxygen species, and vascular remodeling. *Antioxidants & Redox Signaling* 11: 1651-1667, 2009.

8. **Brown TD**. Techniques for mechanical stimulation of cells in vitro: a review. *Journal of Biomechanics* 33: 3-14, 2000.

9. **Carmeliet P**. Manipulating angiogenesis in medicine. *Journal of Internal Medicine* 255: 538-561, 2004.

10. **Carmeliet P**. Mechanisms of angiogenesis and arteriogenesis. *Nature Medicine* 6: 389-395, 2000.

11. **Carosi JA, Eskin SG, and McIntire LV**. Cyclical strain effects on production of vasoactive materials in cultured endothelial cells. *Journal of Cellular Physiology* 151: 29-36, 1992.

12. **Cheng JJ, Wung BS, Chao YJ, and Wang DL**. Cyclic strain-induced reactive oxygen species involved in ICAM-1 gene induction in endothelial cells. *Hypertension* 31: 125-130, 1998.

13. **Chien S, Li, S., Shiu, YT., Li, YS**. Molecular Basis of Mechanical Modulation of Endothelial Cell Migration. *Frontiers in Bioscience* in press, 2004.

14. **Chiu JJ, Usami S, and Chien S**. Vascular endothelial responses to altered shear stress: pathologic implications for atherosclerosis. *Annals of Medicine* 41: 19-28, 2009.

15. **Gade PV, Andrades JA, Nimni ME, Becerra J, Longoria J, Asemanfar N, and Sorgente N**. Nitric oxide mediates hyperglycemia-induced defective migration in cultured endothelial cells. *Journal of Vascular Surgery* 26: 319-326, 1997.

16. **Geiger B, and Bershadsky A**. Exploring the neighborhood: adhesion-coupled cell mechanosensors. *Cell* 110: 139-142, 2002.

17. **Giancotti FG, and Ruoslahti E**. Integrin signaling. *Science, NY* 285: 1028-1032, 1999.

18. **Goldstein BJ, Mahadev K, and Wu X**. Redox paradox: insulin action is facilitated by insulin-stimulated reactive oxygen species with multiple potential signaling targets. *Diabetes* 54: 311-321, 2005.

19. **Gooch KJ**. *Mechanical forces: their effects on cells and tissues*. New York: Springer, 1997.

20. **Hahne JC, Okuducu AF, Sahin A, Fafeur V, Kiriakidis S, and Wernert N**. The transcription factor ETS-1: its role in tumour development and strategies for its inhibition. *Mini Reviews in Medicinal Chemistry* 8: 1095-1105, 2008.

21. **Howard AB, Alexander RW, Nerem RM, Griendling KK, and Taylor WR**. Cyclic strain induces an oxidative stress in endothelial cells. *The American Journal of Physiology* 272: C421-427, 1997.

22. **Hsu PP, Li S, Li YS, Usami S, Ratcliffe A, Wang X, and Chien S**. Effects of flow patterns on endothelial cell migration into a zone of mechanical denudation. *Biochemical and Biophysical Research Communications* 285: 751-759, 2001.

23. **Hynes RO, Bader BL, and Hodivala-Dilke K**. Integrins in vascular development. *Brazilian Journal of Medical and Biological Research = Revista Brasileira de Pesquisas Medicas e Biologicas / Sociedade Brasileira de Biofisica [et al.* 32: 501-510, 1999.

24. **Ingber DE**. Mechanical signaling and the cellular response to extracellular matrix in angiogenesis and cardiovascular physiology. *Circulation Research* 91: 877-887, 2002.

25. **Ingber DE, and Folkman J**. How does extracellular matrix control capillary morphogenesis? *Cell* 58: 803-805, 1989.

26. **Ingber DE, and Folkman J**. Mechanochemical switching between growth and differentiation during fibroblast growth factor-stimulated angiogenesis in vitro: role of extracellular matrix. *The Journal of Cell Biology* 109: 317-330, 1989.

27. **Joung IS, Iwamoto MN, Shiu YT, and Quam CT**. Cyclic strain modulates tubulogenesis of endothelial cells in a 3D tissue culture model. *Microvascular Research* 71: 1-11, 2006.

28. **Kakisis JD, Liapis CD, and Sumpio BE**. Effects of cyclic strain on vascular cells. *Endothelium* 11: 17-28, 2004.

29. **Kitamoto S, and Egashira K**. Endothelial dysfunction and coronary atherosclerosis. *Current Drug Targets* 4: 13-22, 2004.

30. **Madamanchi NR, Hakim ZS, and Runge MS**. Oxidative stress in atherogenesis and arterial thrombosis: the disconnect between cellular studies and clinical outcomes. *Journal of Thrombosis and Haemostasis* 3: 254-267, 2005.

31. **Madamanchi NR, Moon SK, Hakim ZS, Clark S, Mehrizi A, Patterson C, and Runge MS**. Differential activation of mitogenic signaling pathways in aortic smooth muscle cells deficient in superoxide dismutase isoforms. *Arteriosclerosis, Thrombosis, and Vascular Biology* 25: 950-956, 2005.

32. **Mascardo RN**. The effects of hyperglycemia on the directed migration of wounded endothelial cell monolayers. *Metabolism: Clinical and Experimental* 37: 378-385, 1988.

33. **Miao H, Hu YL, Shiu YT, Yuan S, Zhao Y, Kaunas R, Wang Y, Jin G, Usami S, and Chien S**. Effects of flow patterns on the localization and expression of VE-cadherin at vascular endothelial cell junctions: in vivo and in vitro investigations. *Journal of Vascular Research* 42: 77-89, 2005.

34. **Murrant CL, and Reid MB**. Detection of reactive oxygen and reactive nitrogen species in skeletal muscle. *Microscopy Research and Technique* 55: 236-248, 2001.

35. **Penugonda S, Mare S, Goldstein G, Banks WA, and Ercal N**. Effects of N-acetylcysteine amide (NACA), a novel thiol antioxidant against glutamate-induced cytotoxicity in neuronal cell line PC12. *Brain Research* 1056: 132-138, 2005.

36. **Possel H, Noack H, Augustin W, Keilhoff G, and Wolf G**. 2,7-Dihydrodichlorofluorescein diacetate as a fluorescent marker for peroxynitrite formation. *FEBS Letters* 416: 175-178, 1997.

37. **Prosi M, Perktold K, Ding Z, and Friedman MH**. Influence of curvature dynamics on pulsatile coronary artery flow in a realistic bifurcation model. *Journal of Biomechanics* 37: 1767-1775, 2004.

38. **Ruegg C, and Mariotti A**. Vascular integrins: pleiotropic adhesion and signaling molecules in vascular homeostasis and angiogenesis. *Cellular and Molecular Life Sciences* 60: 1135-1157, 2003.

39. **Sastry SK, and Horwitz AF**. Integrin cytoplasmic domains: mediators of cytoskeletal linkages and extra- and intracellular initiated transmembrane signaling. *Current Opinion in Cell Biology* 5: 819-831, 1993.

40. **Schwartz MA, Schaller MD, and Ginsberg MH**. Integrins: emerging paradigms of signal transduction. *Annual Review of Cell and Developmental Biology* 11: 549-599, 1995.

41. **Sheetz MJ, and King GL**. Molecular understanding of hyperglycemia's adverse effects for diabetic complications. *Jama* 288: 2579-2588, 2002.

42. **Shiu YT**. Mechanical forces on cells. In: *Tissue Engineering and Artificial Organs*, edited by Bronzino JD. Boca Raton: CRC Press, 2006, p. 331-3318.

43. **Taniyama Y, and Griendling KK**. Reactive oxygen species in the vasculature: molecular and cellular mechanisms. *Hypertension* 42: 1075-1081, 2003.

44. **Teruyama K, Abe M, Nakano T, Iwasaka-Yagi C, Takahashi S, Yamada S, and Sato Y**. Role of transcription factor Ets-1 in the apoptosis of human vascular endothelial cells. *Journal of Cellular Physiology* 188: 243-252, 2001.

45. **Thornalley PJ**. Glycation in diabetic neuropathy: characteristics, consequences, causes, and therapeutic options. *International Review of Neurobiology* 50: 37-57, 2002.

46. **Wang D, John SA, Clements JL, Percy DH, Barton KP, and Garrett-Sinha LA**. Ets-1 deficiency leads to altered B cell differentiation, hyperresponsiveness to TLR9 and autoimmune disease. *International Immunology* 17: 1179-1191, 2005.